J. Membrane Biol. 75, 141–169 (1983)

The Journal of
Membrane Biology

Interpretation of Current-Voltage Relationships for "Active" Ion Transport Systems: II. Nonsteady-State Reaction Kinetic Analysis of Class-I Mechanisms with One Slow Time-Constant

U.-P. Hansen, J. Tittor*, and D. Gradmann*

Institut für Angewandte Physik, Neue Universität, D-2300 Kiel, Federal Republic of Germany

Summary. The temporal behavior of current through a biological membrane can display more than one time constant. This study represents the reaction kinetic analysis of the nonsteady-state behavior of a class of membrane transporters with one voltage-sensitive reaction step, one dominant (large) time constant, but arbitrary reaction scheme of the voltage-insensitive part of transporter. This class of transporters which shows uniform behavior under steady-state conditions splits into two fundamentally different subclasses, when nonsteady-state behavior is examined: Subclass (Model) A: the slow reaction controls the redistribution of states within the reaction cycle upon an (electrical) perturbation; model B: this redistribution is fast but the transporting cycle can slowly equilibrate with an inactive, "lazy" state. The electrical appearance of model A in a membrane requires specific features of the transporter in the membrane: high densities (10^{-8} mol m^{-2}), low turnover rates (10^3 sec^{-1}) and high stoichiometry ($z>1$) of transported charges per cycle. The kinetics of both models can formally be described by an equivalent circuit with a steady-state slope conductance (G_0) shunted by a (transporter specific) capacitance (G_t) and a conductance (C_t) in series. The voltage dependence of C_t and of G_t can be used to identify model A or model B. In the range of maximum G_0 in the steady-state current-voltage curve, C_t in model A displays a maximum (which may characteristically split into two maxima) and vanishes for larger voltage displacements. C_t can be used for the determination of transporter densities in the membrane. In contrast to model A, the appearance of model B in the nonsteady-state behavior of a membrane does not depend on high densities, low turnover rates and high stoichiometry; it can, therefore, be found also in membranes with sparsely distributed, rapidly transporting channels of any stoichiometry. Particular to model B is a change in the signs of C_t and G_t at the reversal potential of the steady-state current-voltage relationship. This implies switching from capacitive to inductive behavior (under vanishing amplitudes). Also in model B, the nonsteady-state effects disappear for large voltage displacements from the reversal potential. Model B is expected to occur preferably in transporters subject to metabolic control.

Key Words electrogenic pumps · equivalent circuit · inductive behavior · inactive state · nonsteady-state kinetic models · voltage-dependent capacitance

* Max-Planck Institut für Biochemie, Abteilung Membranbiochemie, D-8033 Martinsried, FRG.

I. Introduction

A fundamental constant of biological membranes seems to be the membrane capacitance of about 1 μF cm^{-2}. Since the early measurements of Curtis and Cole (1937) in the cells of the alga *Nitella* and of Curtis and Cole (1938) in squid axons, this value has been confirmed not only in numerous measurements in intact cells of other tissues, but also in reconstituted membranes as that of the isolated protoplasmic drops of *Nitella* (Inoue, Ishima & Horie, 1971).

However, already Blinks and Skow (1941) found "an appreciable polarization component, probably in parallel with a static capacity" in *Valonia*. This is remarkable, because *Valonia* and another seawater alga, *Acetabularia*, recently gave the best experimental support for the phenomena (Tittor, Hansen, Gradmann & Martensen, 1982; Zimmermann, Büchner & Benz, 1982; Tittor, Hansen & Gradmann, 1983), which are related to the deviations from the classical view, and whose theoretical background is discussed in this article. In fact, many impedance measurements in plant cells (Kishimoto, 1974) or in animal cells (Matsumo, Inoue & Kishimoto, 1970) gave strong deviations from the semi-arc expected for the impedance locus of a pure R/C membrane with constant static capacitance.

The results were presented in terms of equivalent circuits with two R/C elements in series or in parallel (Kishimoto, 1974), and interpreted in different ways. For instance, Coster (1973) explained the increase of capacitance of plasmalemma and of tonoplast in *Chara* at low frequencies by diffusion processes. Sandblom, Walker and Eisenman (1972) considered a mobile site membrane, whereas Skierczyńka et al. (1973) postulated an extra membrane. However, Kishimoto et al. (1982) could demonstrate in

perfused *Chara*, that the extra-capacitive element is a property of the plasma membrane alone.

A related effect is the finding of unusually high values of the tonoplast capacitance of *Nitellopsis obtusa* (Findlay, 1970: 2.8 $\mu F/cm^2$) and for the plasmalemma of *Acetabularia* (Gradmann, 1975: 5 $\mu F/cm^2$).

Besides these observations dealing with membrane capacitance, there are other nonsteady-state effects which cannot be explained by the normal action potential mechanism, namely, inductive responses to hyperpolarizing current injections (Kishimoto, 1966; Bradley & Williams, 1967).

In this paper, the above phenomena are taken as indications of the occurrence of nonsteady-state effects of transport systems in the membrane. We assume that it is just a technical reason that the above examples are all taken from electrical measurements, because they provide the required temporal resolution in the msec to sec range (at least for a subclass of these effects). Progress in flux measurement techniques, as for instance ion-selective microelectrodes, (Thomas, 1978) gives hope that in the near future the theoretical model of this paper will become important in a wider field of membrane transport.

Models of nonsteady-state behavior of transporters have been developed for transporters in artificial membranes (Benz & Läuger, 1976; Kolb & Läuger, 1978; Kolb & Frehland, 1980). The approach presented here follows the basic reaction-kinetic concept of these models. However, the models of this paper are adapted to the more complex situation of transporters in biological membranes which implies that a reaction kinetic evaluation of experimental data has to be performed on the basis of incomplete knowledge of the involved reaction scheme, and of limited experimental access.

In a preceding paper (Hansen et al., 1981), it has been shown that such an analysis can be powerful in the case of a certain class of transporters, the so-called Class I transporters. This class consists of all transporters with one pair of reaction constants being sensitive to the driving force under consideration (often membrane potential). In this paper it is shown that this approach can be extended to nonsteady-state behavior with one apparent time constant. However, the uniform Class I of steady-state models splits into two subclasses, which are named model A and model B, when nonsteady-state effects are introduced. In model A, the slow reaction creating the dominant time constant is located within the transport cycle. In model B, the slow reaction is located in a side branch. Model A is similar to the models of artificial membranes cited above, whereas model B generates some new effects. Probably, model B applies to transporters subject to regulation.

II. Steady-State Models of Class I

It has been shown that all transport systems with exactly one pair of reaction constants being sensitive to the driving force under consideration (mostly membrane potential) share the same ensemble of possible flux/driving-force relationships. The curve shapes of these relationships can be described by four apparent reaction constants, independently of how complicated the reaction scheme of the driving force-insensitive reaction constants is. Thus, these transporters can be attributed to a common class, the so-called Class I (Hansen, Gradmann, Sanders & Slayman, 1981).

For current-voltage relationships (I/V curves), the following equation holds:

$$i = zF N_0 \frac{k_{io}\kappa_{oi} - k_{oi}\kappa_{io}}{k_{io} + k_{oi} + \kappa_{io} + \kappa_{oi}} \tag{1}$$

with z, i and F having their usual meanings. N_0 is the total amount of transporters in the membrane. k_{io}, k_{oi}, κ_{io} and κ_{oi} are the reaction constants of a pseudo-2-state model, which has been shown to be able to represent any arbitrary "real" Class I model.

Voltage sensitivity enters Eq. (1) via k_{io} and k_{oi}

$$k_{io} = k_{io}^0 \exp(v/u_T),$$
$$k_{oi} = k_{oi}^0 \exp(-v/u_T) \tag{2a, b}$$

with v being membrane potential, and u_T, the so-called temperature potential, given by

$$u_T = \frac{2RT}{zF}. \tag{3}$$

Equation (4) is based on the assumption that charge translocation by the k reaction constants has to overcome a symmetrical Eyring barrier (Läuger, 1980).

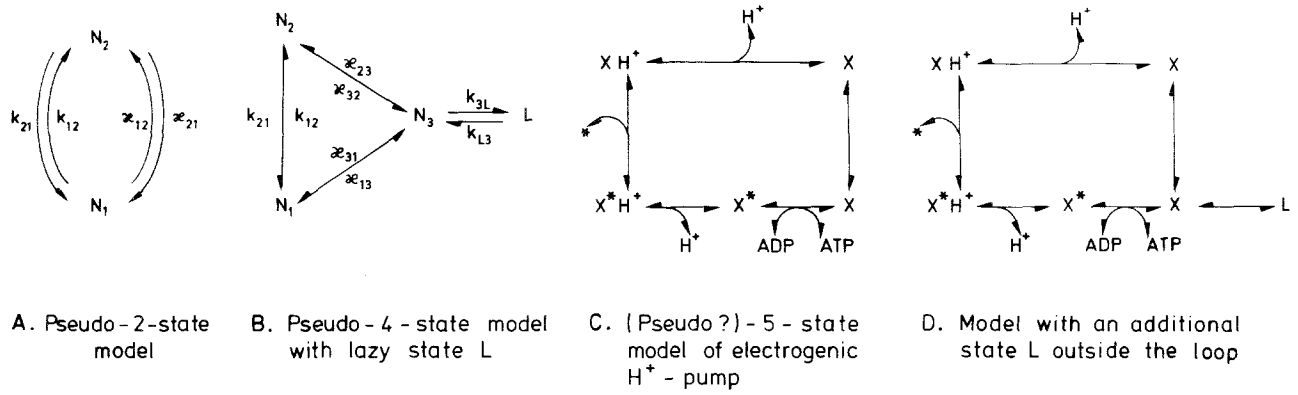

Fig. 1. Different models of Class I transporters. *A.* Pseudo-2-state representation of the scheme in Fig. *C*. The pseudo-2-state model can also represent the reaction schemes of *B* and *D*, if equilibration $N_3 \rightleftharpoons L$ is faster than equilibration within the cycle (premise of model A in this article). *B.* Pseudo-4-state representation of configuration *D*. It has to be used if $N_3 \rightleftharpoons L$ equilibration is slow (premise of model B). *C.* The reaction scheme of an electrogenic pump as assumed for the H^+ pump in *Neurospora* (Hansen et al., 1981). One pair of reaction constants is assumed for each basic function in the transport cycle. However, it cannot be excluded that there are additional states. Thus this model is probably a pseudo-5-state model. *D.* An arbitrary side branch consisting of the lazy state *L* is added to the model of Fig. *C*, thus providing the most general form of a Class I transporter. Such a side branch may be related to regulation of transport activity, if a messenger system controls the $N_3 - L$ conversion (Hansen et al., *in preparation*)

Merging transporters of highly complicated neutral reaction scheme (examples are given by Figs. 1*B*, *C* and *D*) into the pseudo-2-state model of Fig. 1*A* is justified by the theoretical background given by Hansen et al. (1981) and Gradmann, Hansen and Slayman (1982). In general, every chain of chemical reactions can be represented by gross reaction constants (which are called κ in this article), at least under steady-state conditions. Problems arise, when the law of mass conservation is incorporated, because the sum has to comprise all known and unknown states. This problem is circumvented by the usage of so-called reserve factors. The reserve factors assign a multiplicity to the states N_1 and N_2, which originates from the reactions of N_1 and N_2 with the other states of the transporter which do not show up explicitly in Fig. 1*A*. Even though these reserve factors are unknown, they encapsulate the ignorance of the actual reaction scheme in such a nice way, that the greatest possible amount of information can be obtained from given experimental data. Examples of the application of Class I models are given by Gradmann et al. (1982), Hansen et al. (1982), Mummert, Hansen and Gradmann (1981), Sanders and Hansen (1981) and Sanders, Hansen and Slayman (1981).

The introduction of the reserve factors r_1 and r_2 results in the replacement of the "real" gross reaction constants of the "real" *n*-state model (labeled by 1 and 2) by the pseudo-2-state (gross) reaction constants

$$k_{io} = \frac{k_{12}}{r_1}, \quad k_{oi} = \frac{k_{21}}{r_2},$$

$$\kappa_{io} = \frac{\kappa_{12}}{r_1}, \quad \kappa_{oi} = \frac{\kappa_{21}}{r_2}. \qquad (4a, b, c, d)$$

III. Introduction of Nonsteady-State Behavior into Class I Models

The Class I theory outlined above has achieved that stationary kinetic behavior of a major class of membrane transporters can be analyzed straightforward in reaction-kinetic terms. However, improved measuring techniques have enabled recent electrophysiological studies on living systems which gave clear evidence of two time constants in the temporal behavior of biomembranes, of which only one can be attributed to the classical R/C time constant of lipid membranes (Zimmermann et al., 1982; Kishimoto et al., 1982; Tittor et al., 1982, 1983). Thus, analytical tools are required which can investigate the relationship of the nonsteady-state behavior of transport systems to the additionally observed time constant.

Experimental and reaction-kinetic approaches have already been worked out for artificial systems, based on a four-state model (Benz & Läuger, 1976; Kolb & Läuger, 1978;

Kolb & Frehland, 1980). Since rather complex reaction-kinetic networks must be anticipated for transporters in living tissue, the 4-state model cannot *a priori* be assumed to be adequate for the reaction-kinetic analysis of the related phenomena.

The ability of the steady-state Class I approach, as described in section II, to handle a wide class of transporters with arbitrarily complicated reaction-kinetic architecture, is a challenge to extend this approach to nonsteady-state conditions.

For this purpose, we start to treat cases, when one time constant (the largest one) of the system is dominating, such matching the present state of experimental analysis. At the present state, just one time constant can be observed and faster events are still beyond experimental access. Future findings of additional faster time constants will not invalidate this approach, as it is always legal to assume steady-state conditions for reactions which equilibrate faster than the experimental setup can record.

Splitting of Class I into Two Subclasses

The actual reaction schemes of Class I transporters can be highly complicated. The simple loop of Fig. 1 *C* is an example of the reaction schemes usually assumed for electrogenic pumps and cotransporters. However, the existence of side branches cannot be excluded, because steady-state measurements cannot distinguish between the reaction schemes of the kind of Fig. 1 *C* and of the kind of Fig. 1 *D*. As mentioned in section II, the reserve factors mask pecularities of the neutral limb, unless one of these neutral reactions is attacked by a specific drug (Hansen et al., 1981). Side branches of the kind shown in Fig. 1 *D* can be involved in control functions, because transporters in state *L* do not contribute to transport (U.-P. Hansen, D. Sanders & C.L. Slayman, *in preparation*). A similar mechanism has been proposed for the vanadate-trapped state of the (Na, K)-ATPase (Smith, Zinn & Cantley, 1980).

In order to achieve a complete description of nonsteady-state behavior of Class I models with one dominant (largest) time constant, all possible locations of the rate-limiting reaction in a general reaction scheme of Class I transporters have to be taken into account. In this paper it is shown that nonsteady-state Class I models with one time constant display two different modes of behavior which can be attributed to two subclasses of the uniform steady-state Class I model:

Subclass A (also called model A): the slow reaction is located within the main transport cycle. Model A can be represented by the pseudo-2-state model illustrated in Fig. 1 *A*.

Subclass B (model B): the slow reaction is located outside the main cycle (in the side branch). Model B can be represented by the pseudo-3-state model shown in Fig. 1 *B*.

IV. Calculation of the Response of Net Current Through the Transporter to a Change in Membrane Potential

Model A (Slow Reaction Within the Cycle, Fig. 1 A)

The assumption of one rate-limiting step in the neutral recycling limb of the transporter in Fig. 1 *C* or in Fig. 1 *D* enables the representation of the neutral limb by one gross reaction, which leads to the pseudo-2-state model of Fig. 1 *A*. This model is not different from that used for the steady-state analysis (Hansen et al., 1981). Non steady-state behavior results from the process of redistribution of states after a change in driving force.

The following calculations are performed for the net electrical current Δi, as electrical measurements provide the required temporal resolution. However, the results can easily be adapted to flux measurements.

After a change in membrane potential, the voltage-sensitive reaction constants k_{io} and k_{oi} are changed according to Eqs. (2a) and (2b). Now the system starts a relaxation process in order to achieve the new equilibrium. This relaxation process involves transitions of the transporter molecule from one state into another one, and the densities of the two states of the pseudo-2-state model in Fig. 1 *A* are changed according to the following equation

$$r_1 \frac{dN_1}{dt} = (k_{21} + \kappa_{21}) N_2 - (k_{12} + \kappa_{12}) N_1. \quad (5)$$

Equation (5) displays the reaction constants and densities of the "real" n-state model, because fluxes can always be given by the "real" gross- or elementary reaction constants and by the "real" concentrations. The introduction of the reserve factors r_1 and r_2 is required when the

law of mass (transporter) conservation is applied (Hansen et al., 1981).

An effect of this kind leads to the factor r_1 at the left-hand side of Eq. (5). Transporters coming out of N_2 into N_1 immediately spread into all those states which are related to N_1 in Fig. 1 *A* via the reserve factor r_1. Thus the amount of transporters staying in N_1 is smaller than expected from the exchange of N_1 with N_2.

The temporal behavior of model A is calculated in Appendix A on the basis of the relaxation analysis introduced into biology by Eigen (1968). The mathematical evaluation of Eq. (5) leads to the following response of current (or substrate flux) to a stepwise change in membrane potential Δv.

$$\Delta i = \Delta i_\infty + \Delta i_{tA} \exp(-t/\tau_A) \tag{6}$$

with

$$\Delta i_\infty = \frac{zF}{u_T} \cdot \frac{\{k_{io}(k_{oi}+\kappa_{oi}) + k_{oi}(k_{io}+\kappa_{io})\}(\kappa_{io}+\kappa_{oi})}{K^2} N_0 \Delta v \tag{7a}$$

$$\Delta i_\infty = G_0 \Delta v \tag{7b}$$

$$\Delta i_{tA} = \frac{zF}{u_T} \cdot \frac{\{k_{io}(k_{oi}+\kappa_{oi}) + k_{oi}(k_{i\,o}+\kappa_{i\,o})\}(k_{io}+k_{oi})}{K^2} N_0 \Delta v \tag{7c}$$

$$\Delta i_{tA} = G_{tA} \Delta v \tag{7d}$$

$$\tau_A = \frac{1}{K} = \frac{1}{k_{io}+k_{oi}+\kappa_{io}+\kappa_{oi}} \tag{7e}$$

and with u_T given by Eq. (3).

Equation (6) is obtained from Eq. (A17) after adding the two time-independent terms. In Eqs. (7b) and (7d), G_0 and G_{tA} are used as abbreviations for the long expressions in Eqs. (7a) and (7c), respectively. Their relationships to the parameters of the transporter, obtained from the comparison of Eqs. (7a) with (7b) and of Eqs. (7c) with (7d), are listed in Table 1. (Eqs. T1-1, T1-2 and Eqs. T1-5, T1-6). Derivation d/dv of Eq. (1) (compare Eq. A21) shows that G_0 is the steady-state slope conductance of a Class I transporter. Thus Δi_∞ is the steady-state response. This is the reason that, in contrast to Δi_{tA} and G_{tA}, the label "*A*" is omitted, because model A and model B must not be different in steady-state properties (*see* Eq. 12b).

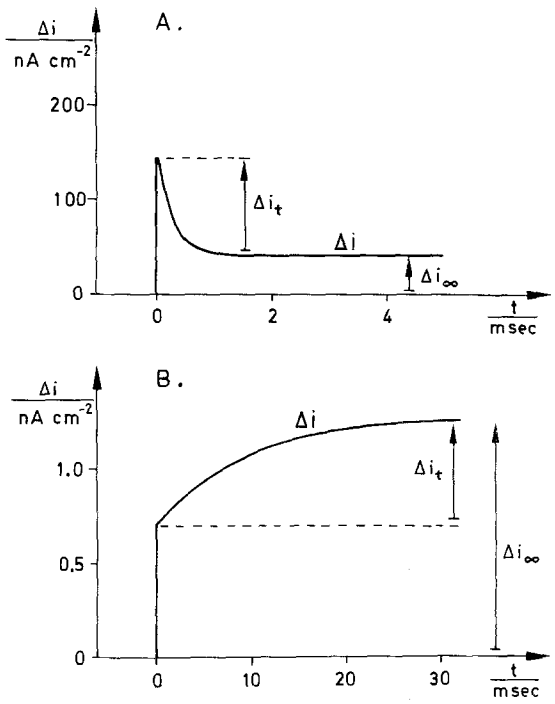

Fig. 2. Responses of the isolated transporter to a step in membrane potential, as given by Eq. (6) and Eq. (11). The responses of current Δi to a step in clamped membrane potential Δv are symmetrical for up- and downward steps in membrane potential, as long as small steps are applied. Small steps are required for the quasi-linear treatment used in this article. *A*. Capacitive behavior: Response of model A (Eq. 6) with the data: membrane potential $= -150$ mV, $z=2$, $E_c=-200$ mV, $N_0=5$ pmol/cm^2, $k^0=\sqrt{k_{io}k_{oi}}=0.5\cdot\kappa_{io}$, $\kappa_{io}=\kappa_{oi}=500\,\mathrm{sec}^{-1}$. Applied step $\Delta v=10$ mV. A similar response is obtained from model B (Eq. 11) in capacitive mode. *B*. Inductive behavior: response of model B (Eq. 11) with similar data as in Fig. *A*, with the exceptions: membrane potential $=-80$ mV, $N_0=1$ pmol/cm$^2\cdot k_{3L}=100\,\mathrm{sec}^{-1}$, $k_{L3}=10\,\mathrm{sec}^{-1}\cdot N_3=N_1$. The scaling factor of the current axis is much smaller in Fig. *B* than in Fig. *A*. This results from the change in N_0 and from the differences in steady-state slope conductance at -150 mV (5 mS/cm^2) and at -80 mV (0.13 mS cm^{-2}). Larger steps Δv would result in nonlinear responses: Model A: For larger nonlinear response the time constant becomes smaller for the step into that direction which points away from the reversal potential of the electrosensitive step (E_c: $k_{io}=k_{oi}$), because of the dependence of τ on v (Eq. 7e). Model B: the dependence of the time constant on voltage (Eq. 12e) is introduced by ρ (Eq. B17) and depends on the actual configuration

Figure 2 *A* displays the time course given by Eq. (6). It consists of an exponential decay with the time constant τ_A and the initial height Δi_{tA} superposed to the steady-state response Δi_∞.

Information That Can Be Obtained from the Nonsteady-State Response of Model A

1. The time constant of the exponential decay in Fig. 2*A* is the inverse of the sum of the pseudo-2-state reaction constants (Eq. 7d). This sum is free of the transporter density N_0. The steady-state approach provides only the unsplitted product of N_0 and the reaction constants. As outlined below, this new feature of the nonsteady-state behavior enables the determination of transporter densities in the membrane.

2. The ratio

$$\frac{\Delta i_{tA}}{\Delta i_\infty} = \frac{k_{io}+k_{oi}}{\kappa_{io}+\kappa_{oi}} \tag{8}$$

is obtained by dividing Eq. (7c) by Eq. (7a). Equation (8) provides a determination of the k/κ ratio, which is independent of the steady-state analysis. Thus it can be used as a test of the applicability of Class I analysis. Such a test gave good results when applied to data obtained from *Acetabularia* (Tittor et al., 1983).

3. The steady-state conductance G_0 (Eqs. 7a and 7b) is already known from steady-state measurements and no special benefit of the nonsteady-state approach.

4. The reaction constants k_{io} and k_{oi} in Eqs. (6) to (8) depend on membrane potential according to Eqs. (2a) and (2b). This voltage-dependence provides an additional source of information and of possible tests of the applicability of this model. However, this discussion is postponed and the behavior of model B is calculated first.

Model B (Slow Reaction Outside the Main Cycle, Fig. 1B)

In contrast to model A, equilibration within the transport cycle is assumed to be very fast. The slow time constant is related to the exchange of the transport cycle with a so-called lazy state L (Fig. 1*D*). The state which exchanges transporters with L is called N_3. The theory of Class I models provides the "right of the most convenient model," and in this case it is the configuration shown in Fig. 1*B*. The reserve factors take care that general validity is maintained (Hansen et al., 1981).

The nonsteady-state behavior results from the following process: After a change in membrane potential, transporters convert from state N_1 to N_2 or vice versa. Due to the assumptions of model B, this equilibration is fast and not observed or ignored by the experimenter. If N_3 is not in the "reaction-kinetic middle" between N_1 and N_2 (*see* factor s_1-s_2 in Eqs. B20, B23 and T2-4), N_3 changes with N_1 and N_2.

Under steady-state conditions, L is tightly connected to N_3 via k_{3L} and k_{L3}. Thus L changes with N_3. But L, N_3 and all other states of the transporter are related by the reserve factors to N_1 and N_2. As these reserve factors stay constant under steady-state conditions, the change in the density of L does not show up explicitly.

Under nonsteady-state conditions, the equilibration of L with N_3 takes time, according to the premise of model B, that the slowest time constant is assigned to this equilibration. Class I theory is constructed around the principle of constant reserve factors (Hansen et al., 1981). Thus, new reserve factors have to be introduced, which exclude L (*see* Eqs. B3a and B3b). The pseudo-2-state reaction constants k'_{oi}, k'_{io}, κ'_{oi}, and κ'_{io} defined on the basis of these new reserve factors (Eqs. B5a to B5d) convert Eq. (1) to

$$i = zF\,\frac{k'_{io}\,\kappa'_{oi} - k'_{oi}\,\kappa'_{io}}{k'_{io}+k'_{oi}+\kappa'_{oi}+\kappa'_{io}}\,(N_0 - L). \tag{9}$$

After a change in membrane potential, the first term changes immediately as the influence of membrane potential on the k reactions is instantaneous (Eqs. 2a and 2b). In the first moment, the value $N_0 - L$ is still that related to the steady state of the previous membrane potential. Thus the resulting current is found outside the steady-state current-voltage curve. Equilibration of L with N_3 causes a relaxation process according to the differential equation

$$\frac{dL}{dt} = k_{3L}\,N_3 - k_{L3}\,L \tag{10}$$

which brings the current back to the steady-state I/V curve. This behavior is discussed in more detail below (Fig. 7).

The mathematical evaluation of Eqs. (9) and (10) is done in Appendix B. For a stepwise change in membrane potential, Δv, the response of current is obtained from Eq. (B26) after the addition of the two time-independent terms

$$\Delta i = \Delta i_\infty + \Delta i_{tB}\exp(-t/\tau_B) \tag{11}$$

with Δi_∞ being identical to Δi_∞ of model A (*compare* Eqs. B24 and B25b with Eq. 7a).

Thus

$$\Delta i_\infty = G_0 \, \Delta v \tag{12a}$$

$$G_0 = G_{0A} = G_{0B}. \tag{12b}$$

As G_{0A} and G_{0B} are identical to the slope conductance of the steady-state I/V curve, G_0 (Eq. T1-2), the indices A and B are omitted.

The nonsteady-state component of Eq. (11), Δi_{tB}, is different from that of model A (Eqs. 6 and 7c):

$$\Delta i_{tB} = \frac{zF}{u_T} \cdot \frac{\{k_{io}(k_{oi}+\kappa_{oi})+k_{oi}(k_{io}+\kappa_{io})\}\,(s_1-s_2)\,i_0}{K\,K_s}\,\Delta v \tag{12c}$$

$$\Delta i_{tB} = G_{tB}\,\Delta v. \tag{12d}$$

The time constant τ_B is no longer related to the reaction constants of the main loop as in Eq. (7e), but to the reaction constants of the $N_3 - L$ exchange.

$$\tau_B = \frac{1}{\rho\, k_{3L} + k_{L3}}. \tag{12e}$$

ρ (Eq. B17), K (Eq. A7) and K_s (Eq. B9) are explained in the appendices. i_0 in Eq. (12c) is the steady-state current calculated from Eq. (1). The coefficients s_1 and s_2 (defined by Eqs. B4a, b) describe the "reaction-kinetic distance" of N_3 from N_1 and N_2, respectively, as seen from Eqs. (B19) and (B20). If s_1 is greater than s_2, N_3 is more tightly bound to N_1 than to N_2, and vice versa.

The responses of model B as given by Eq. (11) are illustrated by Fig. 2*A* and Fig. 2*B*. The responses of model B are identical to those of model A, if the product $(s_1 - s_2) \cdot i_0$ in Eq. (12c) is positive (Fig. 2*A*). However, negative values of this product create a different type of curve shape (Fig. 2*B*) which is called inductive behavior (*see below*).

The product $(s_1 - s_2) \cdot i_0$ changes its sign at the reversal potential of the transporter, when i_0 changes its sign. It cannot be predicted whether inductive behavior is found at higher or lower potentials than the reversal potential, because the sign of the product depends also on $(s_1 - s_2)$ and thus on the actual reaction constants mediating the $N_3 - N_1$ and the $N_3 - N_2$ conversion (*see* Eqs. B13, B19 and B20).

Information That Can Be Obtained from the Nonsteady-State Response of Model B

1. The time constant of the exponential decay (or rise in Fig. 2*B*) provides the sum of the reaction constants of the $N_3 - L$ exchange (Eq. 12e). This sum includes also ρ (defined by Eq. B12a and given by Eq. B17). ρ is a reserve factor describing all unknown states of the transport cycle which exchange with N_3. The occurrence of these reserve factors is the fee for operating with unknown reaction schemes and cannot be avoided when complex systems are investigated. The sum given in the denominator of Eq. (12e) as well as the existence of L at all, is an information which cannot be obtained from steady-state analysis (unless L-specific drugs are used).

2. The ratio

$$\frac{\Delta i_{tB}}{\Delta i_\infty} = \frac{i_0}{(\kappa_{io}+\kappa_{oi})\,N_0} \cdot \frac{K}{K_s} \cdot (s_1 - s_2) \tag{13}$$

is obtained by dividing Eq. (12c) by Eq. (7a). As i_0, the steady-state current, K (Eq. A7), κ_{io} and κ_{oi} are known from steady-state analysis, the ratio s_1/s_2 can be obtained from Eq. (13), and thus the reaction kinetic distance of N_3 from N_1 and N_2.

3. The steady-state conductance G_0 obtained from Δi_∞ by means of Eq. (7b) or Eq. (12b) provides no new insights.

4. The voltage dependence of the parameters of model B can provide new insights as in the case of model A.

V. The Voltage Dependence of the Kinetic Behavior: a Means of Identifying Model A and Model B and of Determining the Optimum Membrane Potential for the Observation of Characteristic Effects

The Usage of an Equivalent Circuit

The coefficients in Eqs. (7a) and (7c) and in Eq. (12c) which give the relationships between the imposed step in membrane potential Δv, and the components of the response in current Δi_∞ and Δi_t, are rather unconvenient. Thus the coefficients were named G_0, G_{tA} and G_{tB} in order to achieve simpler equations (Eqs. 7b, 7d and 12d).

However, the new symbols are more than just handy abbreviations. They have a profound physical meaning: Eqs. (7b), (7d) and (12d)

show that they are conductances (as implied by the symbol G), because they give the ratio $\Delta i/\Delta v$. It has been mentioned already that derivation d/dv of Eq. (1) proves that G_0 is the steady-state slope conductance.

Using the G symbols converts Eqs. (6) and (11) into

$$\Delta i = G_0 \cdot \Delta v + G_t \cdot \exp(-t/\tau) \cdot \Delta v \tag{14}$$

(the indices A and B are omitted, because Eq. (14) applies to model A and to model B).

Equation (14) shows that the current response, Δi, is the sum of the steady-state response and a transient response determined by the transient conductance $G_t \exp(-t/\tau)$. The addition of two currents corresponds to the parallel arrangement of two conductances and leads to the equivalent circuit shown in Fig. 3 *A*.

The transient behavior of Δi_t through G_t given by the exp function is introduced by adding C_t in series with G_t. At the first moment after the step in Δv, C_t is uncharged and the voltage over C_t is zero. Thus the initial current through G_t is the full amount given by Eqs. (7d) and (12d). The current charges C_t, and decreases according to the exp function in Eqs. (6) and (11).

The correct time constant of this process is obtained, if the following values are assigned to C_t:

$$\tau_A = \frac{C_{tA}}{G_{tA}} = C_{tA} \cdot R_{tA} \tag{15a}$$

$$\tau_B = \frac{C_{tB}}{G_{tB}} = C_{tB} \cdot R_{tB}. \tag{15b}$$

A more general approach to the equivalent circuit which holds for any arbitrary curve shape of the imposed input signal Δv, starts from the admittance (inverse impedance) function given by Eq. (A20) for model A and by Eq. (B28) for model B. Comparing these equations with the admittance (conductance) function of the equivalent circuit in Fig. 3 *A*

$$\frac{\overrightarrow{\Delta i}}{\overrightarrow{\Delta v}} = G_0 \frac{1 + p\, C_t/(G_0^{-1} + G_t^{-1})^{-1}}{1 + p\, C_t/G_t} \tag{16}$$

(the arrows indicate complex amplitudes; Riggs, 1966) leads to the same relationships between G_0, G_t and C_t as the above considerations based on step-pulse responses (*see* Tables 1 and 2).

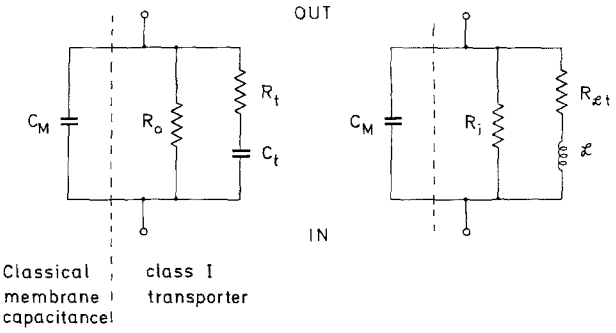

Fig. 3. Equivalent circuits of the nonsteady-state behavior of Class I transporters. *A*. This equivalent circuit applies to all models and modes, if negative values of C_t and R_t are allowed. *B*. If R_t and C_t of circuit *A* are negative, the inductive behavior can be represented by this equivalent circuit. Eqs. (37a–c) convert the elements of circuit *B* to those of circuit *A*. In the text, C_t and $R_t = 1/G_t$ may get additional labels "*A*" or "*B*," when the assignment to one of the two models is to be stressed

Besides the admittance function (Eq. 16), very often the inverse impedance function is used ($R = 1/G$).

$$\frac{\overrightarrow{\Delta v}}{\overrightarrow{\Delta i}} = R_0 \frac{1 + p\, C_t R_t}{1 + p\, C_t (R_0 + R_t)}. \tag{17}$$

If sine waves are used for the analysis, p is related to the frequency f

$$p = 2\pi f \sqrt{-1}. \tag{18}$$

Seeing more behind the symbols G_0 and G_t than just convenient abbreviations of the lengthy terms in Eqs. (7b), (7d) and (12d), and recognizing their relationship to the equivalent circuit in Fig. 3 *A* provides several benefits:

1. At the present state of research, the temporal resolution required for the observation of model A effects can be achieved only by electrical measurements. The natural representation of electrical measurements is the equivalent circuit.

2. The equivalent circuit is the representation of the impedance (Eq. 17) or admittance (Eq. 16) function, which, in contrast to Eqs. (6) and (11), enable the calculation of the responses to any arbitrary input signal (*see* section VII).

3. The impedance function (or admittance function) is well suited for the analysis of sine wave measurements, which are used for this kind of analysis because of the better temporal resolution (e.g. Tittor et al., 1983).

Table 1. Parameters of the equivalent circuit in Fig. 3*A* given in terms of the kinetic data of model A (Fig. 1*A*)

$$R_0 = G_0^{-1} = \left(\frac{di}{dv}\right)^{-1} \quad \text{(T1-1)}$$

$$G_0 = \frac{zF}{u_T} N_0 \frac{\{k_{io}(k_{oi}+\kappa_{oi})+k_{oi}(k_{io}+\kappa_{io})\}\{\kappa_{io}+\kappa_{oi}\}}{(k_{io}+k_{oi}+\kappa_{io}+\kappa_{oi})^2} \quad \text{(T1-2)}$$

$$C_{tA} = \frac{di}{dv} \cdot \frac{1}{\kappa_{io}+\kappa_{oi}} \cdot \frac{k_{io}+k_{oi}}{k_{io}+k_{oi}+\kappa_{io}+\kappa_{oi}} \quad \text{(T1-3)}$$

$$C_{tA} = \frac{zF}{u_T} N_0 \frac{\{k_{io}(k_{oi}+\kappa_{oi})+k_{oi}(k_{io}+\kappa_{io})\}\{k_{io}+k_{oi}\}}{(k_{io}+k_{oi}+\kappa_{io}+\kappa_{oi})^3} \quad \text{(T1-4)}$$

$$R_{tA} = \frac{\tau}{C_{tA}} = \frac{\kappa_{io}+\kappa_{oi}}{k_{io}+k_{oi}} R_0 = \frac{1}{G_{tA}} \quad \text{(T1-5a, b)}$$

$$R_{tA} = \frac{u_T}{zFN_0} \frac{(k_{io}+k_{oi}+\kappa_{io}+\kappa_{oi})^2}{\{k_{io}(k_{oi}+\kappa_{oi})+k_{oi}(k_{io}+\kappa_{io})\}\{k_{io}+k_{oi}\}} \quad \text{(T1-6)}$$

$$\tau_A = \frac{1}{k_{io}+k_{oi}+\kappa_{io}+\kappa_{oi}} \quad \text{(T1-7)}$$

$$N_0 = \frac{u_T}{zF} \frac{(k_{io}+k_{oi}+\kappa_{io}+\kappa_{oi})^3 C_{tA}}{\{k_{oi}(k_{io}+\kappa_{io})+k_{io}(k_{oi}+\kappa_{oi})\}\{k_{io}+k_{oi}\}} \quad \text{(T1-8)}$$

$$q_k = \frac{k_{io}+k_{oi}}{k_{io}+k_{oi}+\kappa_{io}+\kappa_{oi}} \quad \text{(T1-9)}$$

4. The important effects of the classical membrane capacitance C_m and of the conductance of parallel transporters can easily be incorporated.

5. Many experiments indicating nonsteady-state effects (*see* Introduction) are represented in terms of equivalent circuits.

The detailed relationships between the elements of the equivalent circuit in Fig. 3*A* and the reaction kinetic parameters of the transport molecule are listed in Table 1 and in Table 2.

Incorporation of Classical Membrane Capacitance C_m and of the Conductance of Parallel Transporters R_l

In a real membrane, the transporter under investigation is shunted by the classical membrane capacitance C_m and by other transport systems. Equation (19) accounts for C_m:

$$\frac{\overrightarrow{\Delta v}}{\overrightarrow{\Delta i}} = R_0 \frac{1+pR_tC_t}{1+p\{C_t(R_0+R_t)+C_mR_0\}+p^2C_tC_mR_0R_t}. \quad (19)$$

In general, it may be dangerous to mix elements originating from chemical reactions and "real" electrical elements (as C_m) in an equivalent circuit. However, in the case of the transport model considered here, the mixing is legitimate as the reactions of the transport cycle sense membrane potential in the same manner as C_m does. Thus, Eq. (19) and the full equivalent circuit of Fig. 3*A* describe the transporter shunted by C_m properly.

The same considerations can be applied when an ohmic shunt produced by another transporter has to be introduced. In that case, R_0 can be replaced by

$$R_0^* = R_0 \parallel R_l = \frac{R_0 R_l}{R_0+R_l}. \quad (20)$$

As usual in electrophysiology, the index l (leak) denotes all transport systems with which we do not want to deal explicitly.

Restrictions on the Usage of the Equivalent Circuit

The transporter is clearly a nonlinear electrical element. The equivalent circuit in Fig. 3*A* is the quasi-linear representation of its temporal behavior, when it is investigated by means of the relaxation analysis introduced into biology by Eigen (1968). "Linear" implies that the equiva-

Table 2. Parameters of the equivalent circuit in Fig. 3*A* given in terms of the kinetic data of model B (Fig. 1*B*)

$$R_0 = G_0^{-1} = \left(\frac{di}{dv}\right)^{-1} \tag{T2-1}$$

$$G_0 = \frac{zF}{u_T} N_0 \frac{\{k_{io}(k_{oi}+\kappa_{oi})+k_{oi}(k_{io}+\kappa_{io})\}\{\kappa_{io}+\kappa_{oi}\}}{(k_{io}+k_{oi}+\kappa_{io}+\kappa_{oi})^2} \tag{T2-2}$$

$$C_{tB} = \frac{\tau}{R_s} = \tau_B \frac{i_0}{N_0 - L_0} \frac{dL_0}{dv} \tag{T2-3}$$

$$C_{tB} = \frac{zFN_0}{\rho k_{3L}+k_{L3}} \frac{s_1 - s_2}{u_T} \frac{\{k_{io}\kappa_{oi}-k_{oi}\kappa_{io}\}\{k_{io}(k_{oi}+\kappa_{oi})+k_{oi}(k_{io}+\kappa_{io})\}}{\{s_1(k_{oi}+\kappa_{oi})+s_2(k_{io}+\kappa_{io})\}(k_{io}+k_{oi}+\kappa_{io}+\kappa_{oi})^2} \tag{T2-4}$$

$$R_{tB} = \frac{N_0 - L_0}{i_0}\left(\frac{dL_0}{dv}\right)^{-1} = \frac{|i_{sat+}|+|i_{sat-}|}{i_0} \cdot \frac{N_0 - L_0}{N_0} \cdot R_0 = \frac{1}{G_{tB}} \tag{T2-5a, b}$$

$$R_{tB} = \frac{u_T}{zFN_0(s_1 - s_2)} \frac{\{s_1(k_{oi}+\kappa_{oi})+s_2(k_{io}+\kappa_{io})\}\{k_{io}+k_{oi}+\kappa_{io}+\kappa_{oi}\}^2}{\{k_{io}\kappa_{oi}-k_{oi}\kappa_{io}\}\{k_{io}(k_{oi}+\kappa_{oi})+k_{oi}(k_{io}+\kappa_{io})\}} \tag{T2-6}$$

$$\tau_B = \frac{1}{\rho k_{3L}+k_{L3}} \tag{T2-7}$$

$$N_0 = \frac{(\rho k_{3L}+k_{L3})\, u_T \{s_1(k_{oi}+\kappa_{oi})+s_2(k_{io}+\kappa_{io})\}\{k_{io}+k_{oi}+\kappa_{io}+\kappa_{oi}\}^2 C_{tB}}{zF(s_1 - s_2)\{k_{io}\kappa_{oi}-k_{oi}\kappa_{io}\}\{k_{io}(k_{oi}+\kappa_{oi})+k_{oi}(k_{io}+\kappa_{io})\}} \tag{T2-8}$$

$$N_0 - L_0 = \frac{s_1(k_{oi}+\kappa_{oi})+s_2(k_{io}+\kappa_{io})}{k_{io}+k_{oi}+\kappa_{io}+\kappa_{oi}} N_0 \tag{T2-9}$$

$$G_i = G_0 + G_{tB} = \frac{1}{R_0} + \frac{1}{R_{tB}} \tag{T2-10}$$

$$G_i = \frac{zFN_0}{u_T} \frac{\{k_{oi}(k_{io}+\kappa_{io})+k_{io}(k_{oi}+\kappa_{oi})\}\{s_1\kappa_{oi}+s_2\kappa_{io}\}}{\{s_2(k_{io}+\kappa_{io})+s_1(k_{oi}+\kappa_{oi})\}(k_{oi}+k_{io}+\kappa_{oi}+\kappa_{io})} \tag{T2-11}$$

$$s_1 = \frac{r_1 - r_{1L}}{r_1}, \quad s_2 = \frac{r_2 - r_{2L}}{r_2} \tag{T2-12a, b}$$

$$\rho = \frac{N_3}{N_0 - L_0} = \frac{\frac{r_{13}}{r_1}(k_{oi}+\kappa_{oi})+\frac{r_{23}}{r_2}(k_{io}+\kappa_{io})}{s_1(k_{oi}+\kappa_{oi})+s_2(k_{io}+\kappa_{io})} \tag{T2-13}$$

lent circuit predicts the relationships between voltage changes and current changes by a linear impedance function (Eq. 17). "Quasi" implies that the nonlinear behavior enters the analysis via the steady-state voltage dependence of the elements of the transporter or the equivalent circuit (via the k reaction constants (Eqs. 2a, b); *see* Tables 1 and 2). Consequently, the predictions of the equivalent circuit (and of Eqs. 6 and 11) are correct only for small signals superposed to a fixed membrane potential. Wrong results are obtained if this analysis is applied to changes in membrane potential which exceeds the range of constant elements. Therefore, it is absolutely illegitimate to insert d-c batteries into the equivalent circuit and calculate membrane potential or the potential sensed by the elements from Kirchhoff's law.

The Voltage Dependence of the Kinetic Parameters of Model A

Voltage dependence originates from the influence of membrane potential on k_{io} and k_{oi} as given by Eqs. (2a, b). The voltage dependences of $G_0 = 1/R_0$, $G_t = 1/R_t$ and C_t are calculated from the equations in Table 1 for some representative sets of kinetic data of the transporter and displayed in Fig. 4. In addition to the elements of the equivalent circuit, also the steady-state net current i_0, the relative density N_1, and q_k, the ratio of the sum of voltage-sensitive reaction constants to the sum of all reaction constants (Eq. T1-9), are exhibited in Fig. 4. This synopsis provides an understanding of how the voltage dependences of the elements of the equivalent circuit are generated.

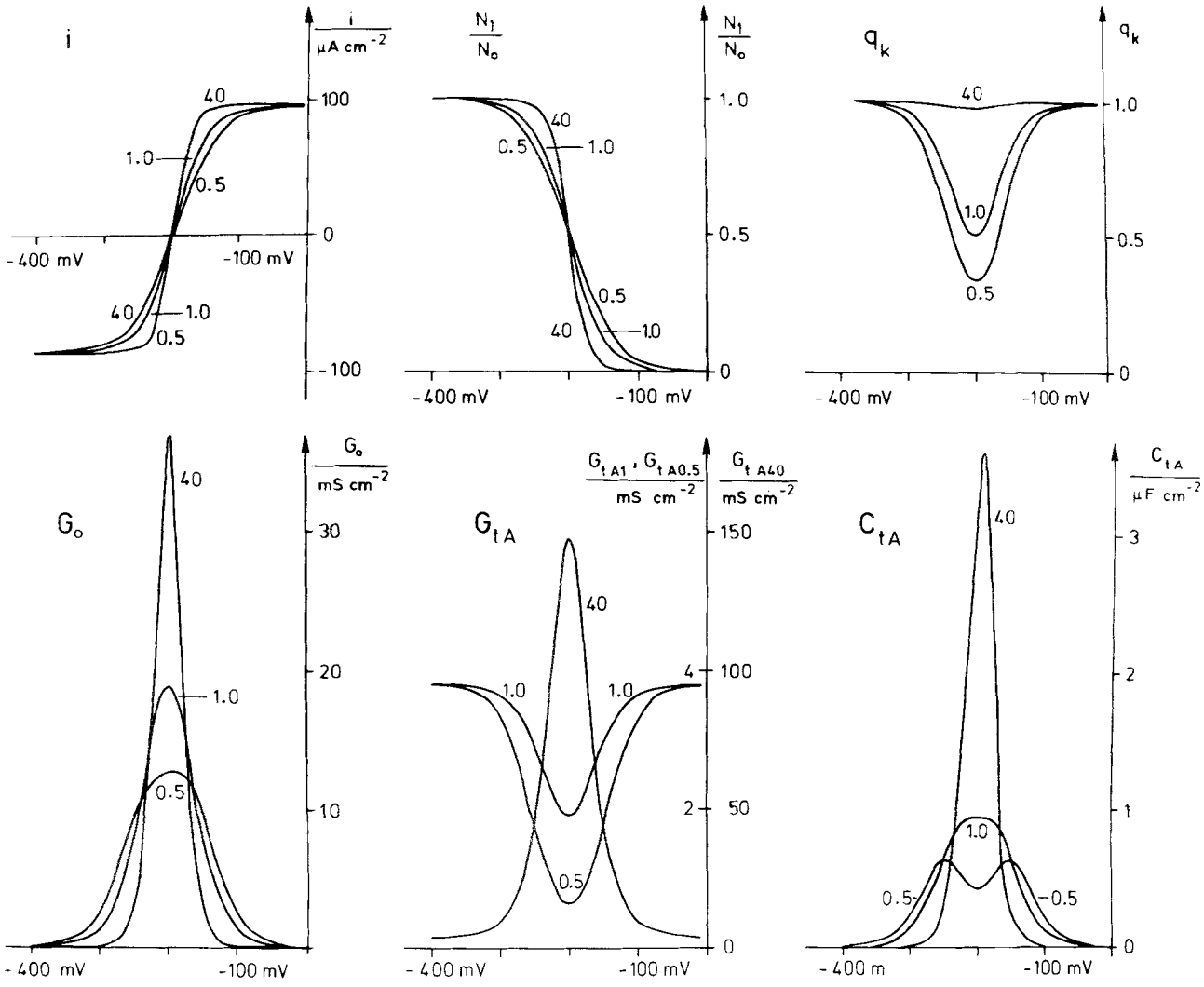

Fig. 4. Model A: Synopsis of the voltage dependences of steady-state current (i_o, Eq. 1), occupation of state 1 (N_1/N_0, Eq. A6a), weighting factor of C_t, in Eq. (T1-3) (q_k, Eq. T1-9), steady-state conductivity (G_o, Eq. T1-2), nonsteady-state conductivity (G_t, Eq. T1-5). The following parameters are common for all three curves in each diagram: $z=2$, $N_0=1$ pmol/cm^2, $\kappa_{io}=\kappa_{oi}=500$ sec^{-1}, $E_c=-200$ mV. The ratio $q=\sqrt{k_{io}k_{oi}/\kappa_{io}\kappa_{oi}}$ is different and indicated by the numbers attached to the curves

A visual inspection of the equations in Table 1 shows that the k/κ ratio influences all equations. Thus the ratio

$$q=\sqrt{\frac{k_{io}\,k_{oi}}{\kappa_{io}\,\kappa_{oi}}}=\sqrt{\frac{k^0_{io}\,k^0_{oi}}{\kappa_{io}\,\kappa_{oi}}} \qquad (21\,\text{a, b})$$

which is independent of membrane potential according to Eqs. (2a, b) is used as a parameter in Fig. 4.

The behavior of the individual elements is as follows:

G_0, the steady-state conductance, needs little comment, because its behavior is already known from the steady-state approach (Hansen et al., 1981; Gradmann et al., 1982). It is displayed in Fig. 4, because it is a major component of C_{tA} in Eq. (T1-3), and because it determines the behavior of Δi_∞ in Eqs. (6) and (11).

G_{tA}, the transient conductance calculated from Eqs. (T1-5) or (T1-6), determines the magnitude of the transient response in Fig. 2A or in Eqs. (6) and (7c). Its dependence on membrane potential is strongly influenced by the k/κ ratio q (Eq. 21). For transporters in which the k reaction constants are much faster than the neutral reaction constants ($q=40$), G_{tA} displays

a sharp peak at the reversal potential of the electrosensitive limb, and can exceed G_0 by a factor of about 4. For q slightly above 1 (not displayed), G_{tA} becomes insensitive to membrane potential. Smaller values of q result in a notch. Thus, G_{tA} at the reversal potential stays significantly below G_0. For instance, for $q=1$ the ratio G_{tA}/G_0 (and also the ratio of Δi_{tA} to Δi_∞ in Fig. 2A) is about 1:10 at the reversal potential. It reaches higher values at a greater distance on the voltage axis, but, as discussed below, this increase does not enhance the chances of observing Δi_{tA}, because in this voltage range C_{tA} vanishes.

C_{tA}, the so-called transporter capacitance, is the most interesting entity as it enables the determination of the transporter density N_0. Its discussion is split into several paragraphs.

C_{tA} and Its Relation to the Determination of the Transporter Density N_0

The ratio $\Delta i_{tA}/\Delta i_\infty = G_{tA}/G_0$ does not provide the transporter density N_0, according to Eq. (8). However, N_0 can be obtained from C_{tA} as seen from the following rearrangement of Eq. (T1-3)

$$C_{tA} = G_0 \frac{zF}{i_{\text{sat}+} + i_{\text{sat}-}} N_0 q_k \tag{22}$$

which leads to the equation for N_0 given by Eq. (T1-8). G_0 is given by Eq. (T1-1), q_k by Eq. (T1-9), and $i_{\text{sat}+}$ and $i_{\text{sat}-}$ are the positive and negative saturation currents ($N_0 \kappa_{oi}$ and $N_0 \kappa_{io}$, respectively, *see* Hansen et al., 1981). These data can be obtained from steady-state analysis. Thus C_{tA} is the relevant parameter which requires the utilization of nonsteady-state analysis for the determination of N_0.

Observability of C_{tA}

The determination of C_{tA} suffers from the fact that the transporter (and thus C_t) is shunted by the classical membrane capacitance of *ca.* 1 μF cm^{-2} (Fig. 3A). Thus C_{tA} is expected to show up in experiments only if it reaches a value of about 1 μF cm^{-2} or more (but *see* discussion of Fig. 10).

As mentioned above, two important factors (besides N_0) determine the magnitude of C_{tA}: the slope of the steady-state I/V curve ($di/dv = G_0$) and a weighting factor q_k (Eq. T1-9).

The maximum slope of the I/V curve depends on the k/κ ratio q (Eq. 21) and is obtained for high q values ($\kappa_{io}\kappa_{oi} \ll k_{io}k_{oi}$). This condition converts Eq. (1) to

$$i - i_{0c} = zF(\kappa_{io} + \kappa_{oi}) N_0 \tanh(v - E_c)/u_T) \tag{23}$$

with i_{0c} being the steady-state current at the reversal potential E_c of the electrosensitive reactions (Hansen et al., 1981; Gradmann et al., 1982). The maximum possible value of $di/dv = G_0$ at E_c is

$$\left(\frac{di}{dv}\right)_{\max} = \frac{zFN_0}{2u_T}(\kappa_{io} + \kappa_{oi}) = \frac{z^2F^2N_0}{4RT}(\kappa_{io} + \kappa_{oi}). \tag{24}$$

The maximum value of the weighting factor q_k (Eq. T1-9) is also obtained for high q values when it becomes equal to "1". This leads to the maximum value of C_{tA} for an optimum transporter (*see* Eq. T1-8):

$$C_{tA\max} = z^2 \frac{F^2 N_0}{4RT} = 0.956\, z^2 \frac{\mu\text{F/cm}^2}{10^{-12}\,\text{mol/cm}^2} \tag{25a, b}$$

with z being the stoichiometry of charge transported per cycle.

Under these optimum conditions (with respect to q), a transporter density in the membrane of 1 pmol/cm^2 or of 0.6 transporters/(10 nm)^2 can generate a capacitance of

$$C_{tA} = 1\,\mu\text{F cm}^{-2} \text{ for } z=1 \text{ or}$$
$$C_{tA} = 4\,\mu\text{F cm}^{-2} \text{ for } z=2. \tag{26a, b}$$

The sign of z is irrelevant, because z is squared in Eq. (25).

Definitions. 1. Transporters which meet the above requirement (high q value: $k_{io}k_{oi} \gg \kappa_{io}\kappa_{oi}$) are called max$-k$ transporters. 2. Transporters with low q values ($\kappa_{io}\kappa_{oi} \gg k_{io}k_{oi}$) are called max$-\kappa$ transporters.

Shifting the Origin of the Voltage-Axis into E_c

The discussion of the influence of membrane potential on the kinetic properties of the transporters can be simplified when instead of the absolute membrane potential v the deviation of v from E_c, the reversal potential of the charge translocating step, is considered:

$$v_d = v - E_c \quad \text{with } E_c = \frac{RT}{zF} \ln \frac{k_{oi}^0}{k_{io}^0}. \tag{27a, b}$$

Introducing Eqs. (27a, b) into Eqs. (2a, b) yields

$$k_{io} = k^0 \exp(v_d/u_T) \tag{28a}$$

$$k_{oi} = k^0 \exp(-v_d/u_T). \tag{28b}$$

In

$$k^0 = \sqrt{k^0_{io}\, k^0_{oi}} = \sqrt{k_{io}\, k_{oi}} = k^0_{io} \exp(E_c/u_T) \tag{29a, b, c}$$

the indices i, o are omitted because at E_c k_{io} and k_{oi} are equal, per definition of E_c.

Equations (28a, b) show that k_{io} and k_{oi}, and thus C_t, R_t and R_0 are completely determined by k^0 (Eq. 29a) and v_d, the distance of the actual membrane potential v from E_c (Eq. 27a).

Symmetry properties which become obvious after this shift of the coordinate system (including a shift of the current axis) have been discussed for the steady-state Class I I/V curve by Hansen et al. (1981). Complete symmetry with respect to E_c is given for $\kappa_{io} = \kappa_{oi}$. Otherwise, the I/V curve is the superposition of two symmetrical curves, an even one and an odd one (thus giving an asymmetrical sum).

The symmetry properties of the steady-state I/V curve enter the nonsteady-state parameters via R_0, the steady-state impedance, in Eqs. (T1-3) and (T1-5b). The additional factors in Eqs. (T1-3) and T1-5b contain k_{io} and k_{oi} only in the symmetrical form $k_{io} + k_{oi}$. Thus R_0 is the only source of asymmetry. This shows that for nonsteady-state behavior, too, symmetry is given for $\kappa_{io} = \kappa_{oi}$.

The Influence of E_c on the Chances of Observing C_{tA} in Max$-k$ Transporters

As shown in Fig. 4 max$-k$ transporters exhibit a sharp peak of C_{tA} at E_c given by Eq. (27b). Thus it is important, that E_c is in the range of possible membrane potentials. Since plasma membranes are usually destroyed at membrane potentials more negative than -300 to -400 mV (Coster, 1965) and at positive membrane potentials, E_c has to be located in the "window" from -400 to 0 mV.

a. Cotransporters. In cotransporters, small values of E_c are expected. An asymmetry in the k^0_{io}/k^0_{oi} ratio can result from asymmetrical reaction constants in the transporter molecule, or from the so-called effect of sensitivity transfer, which converts an asymmetry of the ion gradients into an asymmetry of the k_{io}/k_{oi} ratio via the reserve factors. An effect of this kind is the fundament of Mitchell's "proton motive force" (Hansen et al., 1981). However, it is not assumed that these mechanisms create E_c values which become more negative than -300 mV. A shift of the E_c value to positive potentials would be a very unefficient cotransporter design as it enlarges the difference to membrane potential.

Thus, the chances are high that the C_{tA} peak of a max$-k$ transporter falls into the accessible window at the voltage-axis in the case of cotransporters.

b. Electrogenic Pumps with a Stoichiometry of $z = 2$. (It is more exact to say "with a stoichiometry of 2 charges transported per one ATP split," but usually it is assumed that one transport cycle is performed for 1 ATP split.) If the major part of the free energy of ATP hydrolysis is converted to the $k_{io} - k_{oi}$ asymmetry (as found for *Acetabularia* and for *Neurospora*, Gradmann et al., 1982), then E_c is between -200 and -300 mV. As $z = 2$ favors great values of C_t anyway (Eqs. 25, 26), the chances are very high, to observe reasonable values of C_{tA} in electrogenic pumps with $z = 2$.

Indeed, values of C_{tA} of up to 4 μF cm^{-2} have been found to be associated to the operation of the Cl_2^{2-} pump in *Acetabularia*, even though this pump is not even a clear max-k transporter (Tittor et al., 1983).

c. Electrogenic Pumps with a Stoichiometry of $z = 1$. If the whole free energy of ATP hydrolysis is converted to the k^0_{oi}/k^0_{io} asymmetry, E_c is about -400 to -500 mV. Values of this magnitude have been reported for the H^+ pump in *Neurospora* (Gradmann et al., 1982). Therefore, the maximum value of C_{tA} is outside the "window" of the voltage axis.

The calculation of C_{tA} at the reversal potential of the H^+ pump in *Neurospora* (E_p at about -300 mV) gives an estimate of the magnitude C_{tA} can obtain in a max-k pump with $z = 1$. In *Neurospora*, an asymmetry in the neutral reaction constants (given by $\kappa_{io} \approx 100\, \kappa_{oi}$ and probably resulting from different H^+ concentrations inside and outside the cell (Gradmann et al., 1982)), shifts E_p by 120 mV below E_c resulting in the mentioned value of E_p of about -300 mV. At E_p, the ratio k_{oi}/k_{io} equals κ_{oi}/κ_{io}

$=q_p$. Inserting these conditions into Eq. (T1-3) results in

$$C_{tA} \leqq \frac{z^2 F^2}{2RT} N_0 \frac{2}{q_p} = 0.956 \cdot z^2 \cdot \frac{2}{100} \frac{\mu F/cm^2}{pmol/cm^2}. \quad (30)$$

The "100" in the right-hand denominator demonstrates the difference to Eq. (25). It is seen that C_{tA} of Eq. (30) is expected in the nF cm^{-2} range. This renders its determination very difficult, because it is shunted by $C_m = 1$ μF cm^{-2}. (However, *see* Section VII.)

Even though the slope of the steady-state I/V curve at E_p seems to be close to the limiting steepness of the tanh type (Eq. 23) in *Neurospora*, it is small when compared with the whole span of currents given by the two saturation currents, because the negative saturation current (which usually cannot be measured) is q_p times the visible positive saturation current. Thus it is no surprise that max-k pumps with $z = 1$ cannot create a C_{tA} of reasonable magnitude.

Below it is shown that the max-κ version has a chance of providing greater values of C_{tA}.

The Phenomenon of the Double Peak of C_{tA} in Transporters with Low k/κ Ratios

In Fig. 4 it is seen that C_{tA} displays a new phenomenon when the k/κ ratio q (Eq. 21) falls below 1. For $q = 0.5$, a value corresponding to that found in *Acetabularia* (Tittor et al., 1983), C_{tA} displays a double peak occurring at -140 and -250 mV.

The origin of the formation of the double peak is seen from the comparison of the voltage-dependences of G_0 and q_k (Eq. T1-9) in Fig. 4. For $q = 0.5$, the notch in q_k at E_c becomes stronger than the peak of G_0. Because the double peak is created by a decrease in q_k, it is obvious that the double peaks cannot reach the values of C_{tA} provided by the single peak for $q = 40$. In Fig. 4, the double peaks yield maximum values of C_{tA} which are 1/6 of the optimum value of Eq. (25), but the curve is much broader. Nevertheless, these conditions still can produce values of C_{tA} which are sufficiently large for the detection in living membranes. Such a double peak has been observed in experiments on the Cl_2^{2-} pump of *Acetabularia* (Tittor et al., 1983).

The locations and the relative heights of the two peaks can be calculated from the derivation dC_t/dv very easily, when the two peaks are well separated. As mentioned above, the single peak is always located at E_c. The two peaks move away from E_c, when q is lowered. Because of the steep dependence of k_{io} and k_{oi} on membrane potential (Eqs. 2a, b and 28a, b) the peaks soon reach the regions for which the following conditions hold: $k_{io} \gg k_{oi}$ at the positive side of E_c, and $k_{oi} \ll k_{io}$ at the negative side. In that case, the locations of the two peaks are about symmetrical to E_c, namely at potentials defined by the relationships:

$$k_{io} \approx \frac{k_{io} k_{oi}}{\kappa_{io} + \kappa_{oi}} \quad \text{or} \quad k_{oi} \approx \frac{k_{io} k_{oi}}{\kappa_{io} + \kappa_{oi}}. \quad (31\text{a, b})$$

The introduction of these conditions into Eq. (T1-4) leads to

$$\frac{C_{tA\,\max\,pos}}{C_{tA\,\max\,neg}} = \frac{\kappa_{oi}}{\kappa_{io}}. \quad (32)$$

The Influence of E_c on the Chances of Observing C_{tA} in Max-κ Transporters

a. Cotransporters and electrogenic pumps with a stoichiometry of $z = 2$ have the best chances of creating high values of C_{tA} for max-k transporters, as discussed above. This holds also for max-κ transporters and for transporters with q values (Eq. 21) of about 1, because at least one of the two peaks should fall into the accessible voltage range. The example of *Acetabularia* mentioned above is the experimental verification of this expectation.

b. Electrogenic pumps with a stoichiometry of $z = 1$ (E_c about 450 mV) are not able to generate high values of C_{tA} in the case of max-k transporters (Eq. 30), because the location of maximum C_{tA}, E_c, is beyond the range of accessible membrane potentials. The phenomenon of the double peak which occurs in max-κ transporters can move one of the peaks down to the more favorable range of membrane potentials.

The conditions $\kappa_{io} < \kappa_{oi}$ and $\kappa_{oi} \gg \sqrt{k_{io} k_{oi}} = k^0$ and $k_{io} \gg k_{oi}$ (because of the distance from E_c) convert Eq. (T1-4) to

$$C_{tA} = \frac{z^2 F^2}{2RT} N_0 \frac{\kappa_{io} k_{io}^2}{(\kappa_{oi} + k_{io})^3} \quad (33)$$

which reaches its maximum value at $\kappa_{oi} = k_{io}/2$. Thus

$$C_{tA\,\max} = 0.956\, z^2 N_0 \frac{1}{6.75} \frac{\mu F/cm^2}{pmol/cm^2}. \quad (34)$$

This $C_{tA\,max}$ value is smaller only by a factor of 6.75 than the optimum one for a max-k transporter with $z=2$ (Eq. 25). This is of similar magnitude as the factor 1/6 for $C_{tA\,max}$ of the double peaks of the curve for $q=0.5$ in Fig. 4. These conditions lead to $4\,\mu F\,cm^{-2}$ in *Acetabularia* (Tittor et al., 1983) as mentioned above. Even though $C_{tA\,max}$ in a $z=1$ transporter is smaller by a factor of 4 because of z^2 in Eqs. (25) and (34), a value of $C_{tA\,max}=1\,\mu F\,cm^{-2}$ could show up.

However, the conditions which lead to the max-κ type discussed above are very strange: The condition $\kappa_{oi}>\kappa_{io}$ moves the reversal potential of the pump E_p to even more negative potentials. That is the opposite of what is found in *Neurospora* (Gradmann et al., 1982). Membrane potential may be still at normal values of -200 mV, since the I/V curve (Fig. 5) is very flat until it starts to increase. Thus a leak could easily bring membrane potential down to the region of maximum slope. However, the great difference between E_p and membrane potential would be a waste of energy.

The flatness of the I/V curve results from the condition $\kappa_{oi}\gg\sqrt{k_{io}k_{oi}}$ which shifts the steep part of the I/V curve (G_0 as a factor of C_{tA} in Eq. T1-3) down into the range of accessible membrane potentials.

Electrogenic pumps of the above max-κ type have not been identified so far. Adequate conditions may be created by low inside concentrations of the transportee (for a positive ion) which make κ_{io} very small, and by lowering the k reaction constants by poisoning. Under these conditions it should be checked whether C_{tA} shows up.

The voltage dependences of membrane current i_0, relative density of N_1, q_k (Eq. T1-9), C_{tA}, G_{tA} and G_0 are displayed in Fig. 5 for a transporter which meets the above requirements.

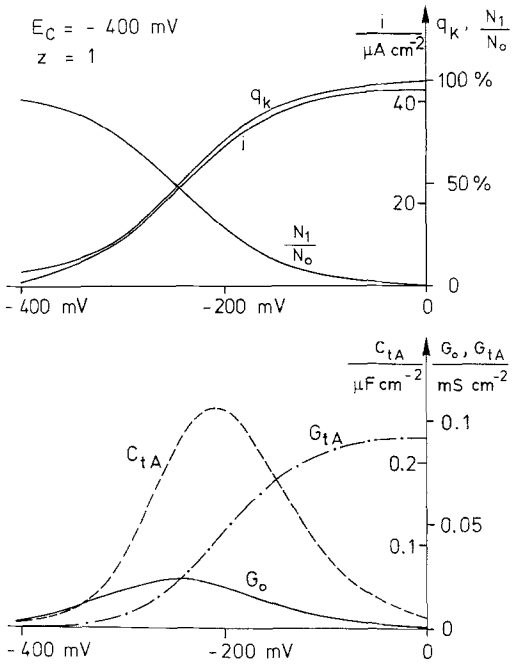

Fig. 5. Model A: Voltage dependences of i_0, N_1/N_2, q_k, G_0, G_t and of C_t as in Fig. 4, but for a pump with a stoichiometry of 1 ion transported/1 ATP split ($z=1$), and the following kinetic data: $E_c=-400$ mV, $\sqrt{k_{io}k_{oi}}=\kappa_{io}=0.05\,\kappa_{oi}$, $\kappa_{oi}=500\,sec^{-1}$, $N_0=1$ pmol/cm^2

The Double Peak of C_{tA} as a Means of Distinguishing Between Competing Steady-State Models

In an actual biological membrane, where a parallel "leak" can draw the left-hand side of the I/V curve below the voltage axis, it can be difficult to decide from a measured I/V curve whether a 2:1 or 1:1 stoichiometry is given, especially if the "window" on the voltage axis is narrow. In such a situation, the finding of a double peak of C_{tA} can rule out the 1:1 stoichiometry, because the double peak is centered around E_c.

The Voltage Dependence of the Kinetic Parameters of Model B

Figure 6 displays the voltage dependences of max-k and of max-κ transporters for the data sets given in the legend. There are two features which differ strongly from the behavior of model A.

1. C_t of model B (C_{tB}) can be orders of magnitude greater than C_{tA}.
2. C_{tB} changes its sign when the current i_0 through the transporter changes its sign at E_p, the reversal potential of the pump.

The Independence of the Occurrence of C_{tB} on High Transporter Densities N_0

The magnitude of C_{tB} originates from a very important feature: C_{tB} is independent of N_0. This is not true in absolute terms. However, for a given current i_0, it does not matter, whether it is achieved by high reaction constants (namely κ) or by high values of N_0. If i_0 is given, C_{tB} no longer depends on N_0 which occurs in

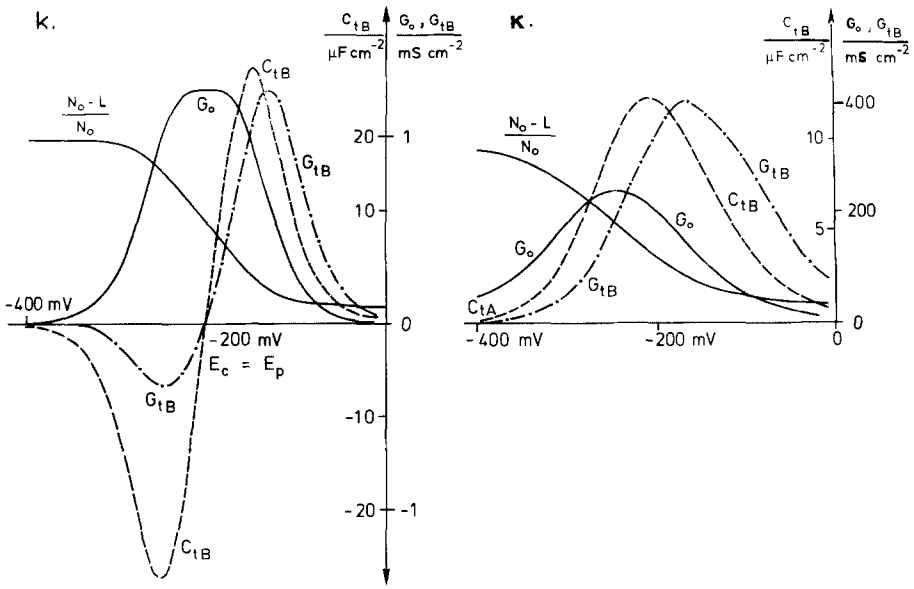

Fig. 6. Model B: Voltage dependence of the ratio of active transporters $(N_0 - L)/N_0$, Eqs. T2-8 and T2-9), steady-state conductivity (G_0, Eq. T2-1 or Eq. T2-2), nonsteady-state conductivity (G_t, Eq. T2-6) and of pump capacitance (C_t, Eq. T2-4). *k:* Same data as in Fig. 4, curve "0.5" (still a max-*k* type). *κ*: Same data as in Fig. 5 (max-*κ* type). The steady-state *I/V* curves are identical to those in Fig. 4 ("0.5") and in Fig. 5, respectively

$(N_0 - L_0)$ and in dL_0/dv in Eq. (T2-3). In addition, C_{tB} can be brought to any arbitrary value by an adequate selection of k_{3L} and k_{L3}.

The independence from N_0 implies that not only transporters with low turn over rates and consequently high densities as in the case of model A, but all kinds of transporters including channels with very high turnover rates and low densities can generate high C_t values.

The chances of observing the nonsteady-state behavior do not only depend on C_t alone. Equation (12) indicates that the ratio of transient to steady-state current ($\Delta i_t/\Delta i_\infty$, *see* Fig. 2) which is given by G_t/G_0 (*see* Eqs. 12a and 12d) should be favorable. Equation (T2-5b) demonstrates that this ratio depends on the factor $N_0/(N_0 - L_0)$. From this factor it is concluded, that a major part of the transporters has to be in the lazy state L in order to give distinct signs of the nonsteady-state effects. (This is obvious: state L can only show up if it is populated.)

The Change in Sign of C_{tB}

The change in sign in C_{tB} is the most exciting feature of model B. In Eqs. (T2-3) and (T2-4), two parameters determine the sign of C_{tB}, namely $(s_1 - s_2)$ and the current i_0. $(s_1 - s_2)$ is not voltage dependent and related to the reaction scheme of the transporter (*see* Eqs. B4 and B19). If N_3 is more tightly bound to N_1, then s_2 is greater than s_1, and vice versa.

Positive C_{tB} results from the following mechanism: The state from which transport of positive charge starts is called N_1 (as always in this article). A positive increase in membrane potential promotes the conversion of N_1 to N_2. $s_2 < s_1$ implies that N_3 is reaction-kinetically closer to N_2 than to N_1. Thus N_3 increases with N_2. As N_3 equilibrates with L, transporters move into the inactive state L, and current decreases after an initial rise (Fig. 2*A*). This process creates capacitive behavior.

If $s_1 < s_2$, then N_3 senses the decrease of N_1 instead of the increase in N_2, and transporters come out of L. This results in an increase of current and thus in inductive behavior according to Fig. 2B.

The above considerations hold for membrane potentials more positive than E_p. At potentials more negative than E_p, $s_2 < s_1$ creates inductive behavior and $s_1 < s_2$ capacitive behavior.

An Illustration of the Generation of Inductive or Capacitive Behavior

The mechanism of the generation of capacitive or inductive behavior is illustrated in Fig. 7. Fig. 7O shows a configuration with L directly coupled to N_2 ($N_3 = N_2$, $r_{1L} = 0$, $s_1 = 1$, $s_2 < s_1$ according to Eqs. B3 and B4). In Fig. 7I, L is directly coupled to N_1 ($N_3 = N_1$, $s_1 < s_2$). The steady-state *I/V* curves of both configurations are identical and equal to that in Fig. 4, curve 1.0 (but with fivefold value of N_0). The second curves cannot be measured under steady-state conditions. They are calculated from

$$i_{ns(v)} = zF w_{(v+\Delta v)}(N_0 - L)_{(v)} \tag{35}$$

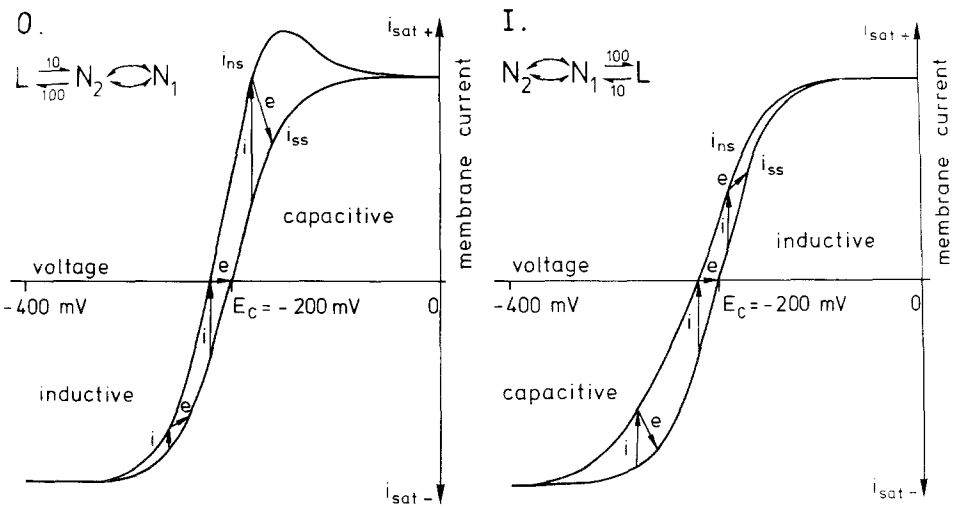

Fig. 7. Illustration of the generation of capacitive and inductive behavior. i_{ss} (steady state) is calculated from Eq. (1) and identical to that of Fig. 4, curve "1.0". i_{ns} is the nonsteady-state current calculated from Eq. (35). It is observed, when membrane potential is suddenly shifted by 20 mV towards positive potentials. The rate constants adjust immediately to the new potential, whereas $N_0 - L$ still keeps its old value. The arrows "i" (initial) and "e" (equilibration) give a rough estimate of the time course of the response of current (*see* Fig. 2). I: L exchanges with N_1 only ($N_3 = N_1$); O: L exchanges with N_2 ($N_3 = N_2$). Common data: $z = 2$, $\sqrt{k_{io} k_{oi}} = \kappa_{io} = \kappa_{oi} = 500\ \text{sec}^{-1}$, $E_c = -200$ mV, $N_0 = 1$ pmol/cm^{-2}, $k_{3L} = 100\ \text{sec}^{-1}$, $k_{L3} = 10\ \text{sec}^{-1}$

with w being defined by Eq. (B1b). Equation (35) differs from Eq. (B1b) by the differences in the potentials v and $v + \Delta v$ to which $(N_0 - L_0)_{(v)}$ and $w_{(v+\Delta v)}$ are assigned.

Equation (35) applies to an experiment as follows: The transporters have reached steady state. Then, the step Δv is applied, e.g. by a voltage-clamp circuit. The reaction constants included in w immediately switch to their new values ($w_{(v+\Delta v)}$), but the exchange of L with the cycle has just begun to adjust to the new distribution of N_1 and N_2. Thus the old value of $(N_0 - L)_{(v)}$ occurs in Eq. (35).

The arrows in Fig. 7 give a rough picture of the time course of membrane current (*compare* Fig. 2A and Fig. 2B). The arrow "i" indicates the initial upward deflection of the current resulting from the immediate change in w. The arrow "e" (equilibration) gives (at least the direction of) the change in current resulting from the equilibration of L with the cycle and its effect on the number $(N_0 - L)$ of active transporters. Arrow "e" ends on the steady-state curve as expected.

The ratio of curvatures of the steady-state and of the nonsteady-state I/V curves determines whether the arrows "i" and "e" point into the same direction (inductive behavior) or into opposite directions (capacitive behavior). At E_p, an ohmic response is observed according to the result of Fig. 6*k* that C_{tB} is zero at the reversal potential of the transporter.

VI. Stability and Oscillations in Model B

The occurrence of negative elements in an equivalent circuit always raises the question of stability. Astability is given, if a pulse at the input port leads to a response which does not return to the steady-state value. This would happen, if the time constant τ_B in Eq. (11) would be negative. As noise can generate pulses in Δi and in Δv, stability has to be checked separately for the responses of Δi to Δv (applying to voltage-clamp conditions: stability of admittance) and for the response of Δv to Δi (applying to open loop conditions, e.g. in the living cell: stability of impedance).

A. Stability of Admittance (Voltage Clamp)

Stability of conductance is given, if τ_B in Eq. (11) is positive. The positive sign of τ_B is guaranteed by Eq. (12e), as k_{3L} and k_{L3} are always positive. However, τ_B is also given by Eq. (15b) which seems to indicate that τ_B changes its sign with C_{tB}. The solution is found by the inspection of Eqs. (T2-3) and (T2-5a): C_{tB} and R_{tB} change their signs simultaneously at E_p. Thus the product $C_{tB} R_{tB}$ in Eq. (15b)

stays always positive and stability is given at all membrane potentials.

B. Stability of Impedance (Open Loop)

The equation $\Delta v/\Delta i$ which corresponds to Eq. (11) is given below (Eq. 46). However, stability can also be checked on the basis of the impedance function ($\overrightarrow{\Delta v}/\overrightarrow{\Delta i}$) given by Eq. (17) or by Eq. (B28), because the relevant time constant τ_{nB} occurs in the denominator of the impedance function.

Testing the sign of τ_{nB} can start from two different equations, namely Eq. (B30) giving the relationship of τ_{nB} to the parameters of the transporter, or Eq. (B32) expressing τ_{nB} in terms of the equivalent circuit.

Equation (B30) shows that τ_{nB} is positive at all membrane potentials, because all factors in Eq. (B30) are positive. Thus the impedance function is stable.

Equation (B32) provides positive values of τ_{nB}, if $-R_{tB}$ is greater than R_0, if R_t is negative, because in this case the negative sign of $(R_{tB}+R_0)$ cancels the negative sign of C_{tB}. This could be shown by a laborous evaluation of Eqs. (T2-2) to (T2-6). Instead, we use the knowledge of stability gained from Eq. (B30) in order to conclude that $-R_{tB}$ is greater than R_0 under conditions which render $R_{tB}<0$.

Relationships Between the Frequency Responses of Amplitude and of Phase

Because τ_{nB} occurs in the numerator of Eq. (B28), it is called a zero. A positive zero implies that Eq. (B28) describes a minimum-phase function. This is an important statement for the experimenter: In minimum-phase networks investigated by means of sine waves, the frequency response of the amplitude determines completely the frequency response of the phase, and vice versa (Bode, 1964). Thus, the experimenter needs to measure only one of the frequency responses, or can use the measurement of both as a powerful test of the reliability.

As τ_B and τ_{nB} are both positive, the properties of stability and of minimum phase are guaranteed for the conductance function (Eq. B28, voltage clamp) as well as for the inverse impedance function (open loop).

An Alternative Equivalent Circuit of Model B Describing Inductive Behavior

The equivalent circuit of model B and of model A is given by Fig. 3*A*. It holds for capacitive and for inductive behavior. However, the occurrence of negative elements should be avoided if possible. The adequate equivalent circuit of inductive behavior is shown in Fig. 3*B*. Its admittance (conductance) function is

$$\frac{\overrightarrow{di}}{\overrightarrow{dv}}=\{G_i+G_{lB}\}\frac{1+p\,\mathrm{L}\left(\frac{1}{G_i}+\frac{1}{G_{lB}}\right)^{-1}}{1+p\,\mathrm{L}\,G_{lB}}. \tag{36}$$

This impedance function looks similar to Eq. (16) and is related to the elements of the equivalent circuit in Fig. 2*A* of Eq. (16) as follows:

$$G_i=G_0+G_{tB} \tag{37a}$$

$$G_{lB}=-G_{tB} \tag{37b}$$

$$\mathrm{L}=-C_{tB}\frac{1}{G_{tB}^2}. \tag{37c}$$

Obviously, the difference of capacitive and inductive behavior cannot result from the usage of the symbols L instead of C_{tB} or of G_i (initial conductivity) and G_{lB} instead of G_0 and G_{tB}. As discussed in more detail below, the important feature is the relative location of the roots of the numerator and of the denominator of Eq. (36) (or of Eq. 16).

The Occurrence of Oscillations in a Membrane with a Model B Transporter

The equivalent circuit of Fig. 3*B* looks like a resonance circuit, when the transporter is shunted by the classical membrane capacitance C_m. (The conductances of other transporters are ignored as they can easily be incorporated via Eq. 20.)

The occurrence of oscillations depends on the damping factor. It can be calculated from the impedance function of the transporter shunted by C_m as given by Eq. (19). By calculating the roots of Eq. (19), the impedance function can be presented in a standard form

$$\frac{\overrightarrow{d\Delta v}}{\overrightarrow{d\Delta i}}=R_0\frac{1+p\tau_B}{(1+p\tau_1)(1+p\tau_2)} \tag{38}$$

with

$$\tau_{1/2}=\frac{R_0(C_m+C_t)+R_t C_t}{2}\pm\sqrt{\frac{(R_0(C_m+C_t)+R_t C_t)^2}{4}-R_0 R_t C_m C_t}. \tag{39}$$

Table 3. Synopsis of the properties of nonsteady-state behavior of model A and of model B

	Model A	Model B
expected occurrence	pumps, contransporters with low turnover rates	pumps, cotransporters, channels: low and high turnover rates
origin of time constant	rearrangement within the transport cycle	exchange with sidebranch (regulation)
simplest reaction scheme	one cycle	cycle with side branch
lowest required	$z=2$: 0.25 pmol/cm^2	free
density	$z=1$: 7 pmol/cm^2	
favorite stoichiometry	$z \geqq 2$	free
stability	always given	always given
oscillations	none	rare, damped
quality influencing phenotype	k/κ-ratio q	relative coupling of N_3 to N_1 and N_2
type of response	capacitive	capacitive or inductive
peculiarities	double peak of C_t at low q	change in sign of C_t at E_p
experimental evidence	Tittor et al., 1983; Zimmermann et al., 1982; Kishimoto et al., 1982; Gradmann, 1975; Blinks and Skow, 1941	weak: Kishimoto, 1966; Bradley and Williams, 1967; Ohkawa and Kishimoto, 1974

Oscillations occur if $\tau_{1/2}$ become complex numbers. The admittance function (voltage-clamp conditions) cannot show oscillations, as the denominator of the inverse of Eq. (38) is only of first degree.

However, the impedance function, Eq. (38), can create complex time constants. An example is given by Fig. 9*e* at potentials more negative than -325 mV (the inherent symmetry implies that in the other configuration, $N_3=N_1$, where inductive behavior is found at the positive side of E_p, the complex time constants occur at potentials more positive than -65 mV).

Other data sets (e.g. $q=10$ (Eq. 21), $\kappa_{oi}=\kappa_{io}$, $N_0=10^{-12}$ moles/cm^{-2}, $z=2$, k_{3L} and k_{L3} as in Fig. 9*e*) give isolated ranges of complex time constants (in the example: from -280 to -330 mV for $N_3=N_2$, and from -70 to -120 mV for $N_3=N_1$).

The damping of these oscillations is very strong. Fig. 9*e* shows that the imaginary component of τ_1 and τ_2 ($\mathrm{Im}\,\tau_{1/2}$) is always smaller than the real one ($\mathrm{Re}\,\tau_{1/2}$). Only at -370 mV, the imaginary component touches the real one. The ratio of the two components determines the damping factor which is worse than 1 according to Fig. 9*e*.

Using the above finding that $|R_{tB}|>|R_0|$ in the inductive range and the relationship $a^2+b^2 \geqq 2ab$, leads to the general statement that the real component of Eq. (30) is always greater than the imaginary one.

Consequently, the inductive model B can create oscillations, but they damp out rapidly.

Survey of the Properties of Model A and of Model B

In Table 3 the properties of the two models are summarized.

VII. Applications: The Influence of the Choice of Input Signal and of Input Port on the Chances of Observing Nonsteady-State Behavior of Model A and of Model B

The Choice of the Input Port: Voltage Clamp or Current Clamp

Kinetic measurements of transporter behavior can be done under voltage-clamp or under open-loop conditions (current clamp). The first method corresponds to the admittance (conductance) function $\overrightarrow{\Delta i}/\overrightarrow{\Delta v}$ given by Eq. (16) for the isolated transporter or by the inverse of Eq. (19) for the transporter embedded in the membrane. The second method corresponds to the impedance function $\overrightarrow{\Delta v}/\overrightarrow{\Delta i}$, given by Eq. (17) or by Eq. (19). It is shown below that the two methods yield very different efficiencies when step functions are used as input signals.

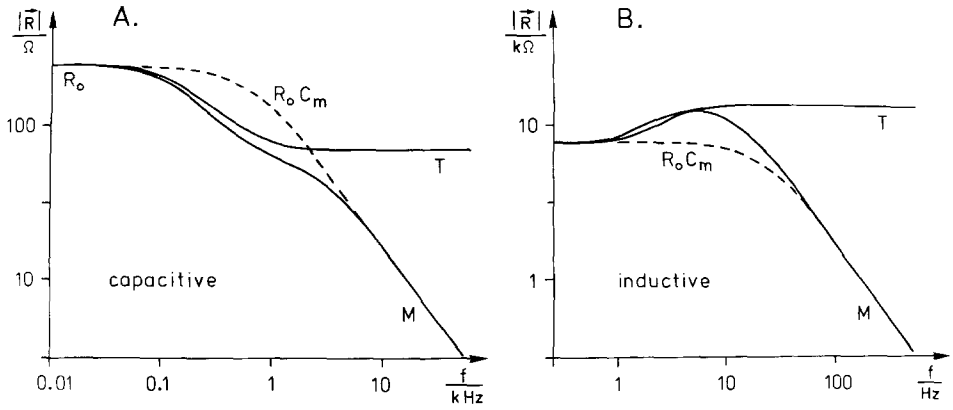

Fig. 8. Frequency responses of the amplitude of electrical impedance R, calculated from Eq. (40) for the isolated transporter (T) and from Eq. (41) for the transporter embedded in the membrane (M). $R_0\,C_m$ gives the frequency responses of a pure R/C membrane. *A*. Capacitive behavior displayed by model A with the data given in Fig. 2*A*. Potential is assumed to be -150 or -250 mV, where the distances of τ_A to τ_1 and to τ_2 attain maximum values (*see* arrows in Fig. 9*c*). Similar frequency responses are obtained from model B in capacitive mode. *B*. Inductive behavior displayed by model B with the same data as in *A*, but $N_0 = 1$ pmol/cm^{-2}, corresponding to Figs. 2*B*, 6*k* and 9*e*. Membrane potential is -320 mV for the configuration $N_3 = N_2$, or -80 mV for the configuration $N_3 = N_1$

The Choice of the Input Signal: Sine Waves or Step Functions

The theory of linear (or quasi-linear, as in this article) networks implies that the knowledge of the response obtained by a certain input signal enables the calculation of the responses to any other input signal (Bode, 1964; Riggs, 1966). Thus, from a theoretical point of view, the selection of the input signal should be of little importance.

However, this is correct only if the measurements can be performed with infinite accuracy. Biological systems are far away from this premise. In this section, the particular advantages of two important input signals are compared: sine waves and step functions.

Sine Waves

Sine waves have been used for biological impedance measurements since the early beginnings of electrophysiology (reviewed by Cole, 1968). The results are presented by the dependence of amplitude and of phase shift φ on the frequency f of the applied sine wave. Usually, complex numbers ($\vec{R} = |R| \exp(\varphi \sqrt{-1})$) are used in order to merge both functions into one. Equations (16), (17), (19) and (38) are complex frequency responses of this kind.

The frequency response of the isolated transporter is obtained from Eq. (17) ($p = 2\pi f \sqrt{-1}$):

$$\frac{\vec{\Delta v}}{\vec{\Delta i}} = \vec{R}_T = R_0 \frac{1 + p\tau}{1 + p\tau_n} \tag{40}$$

that of the transporter embedded in the membrane from Eq. (19):

$$\frac{\vec{\Delta v}}{\vec{\Delta i}} = \vec{R}_M = R_0 \frac{1 + p\tau}{(1 + p\tau_1)(1 + p\tau_2)}. \tag{41}$$

R_0 in Eq. (41) may include the conductivities of parallel transport system in the membrane according to Eq. (20).

The indices A and B are omitted in Eqs. (40) and (41) because the considerations hold for both models. τ is given by Eqs. (15a) or (15b) (or by Eqs. T1-7 or T2-7); τ_n, obtained from the denominator of Eq. (17) is

$$\tau_n = C_t(R_0 + R_t) \tag{42}$$

or given by Eqs. (A27) and (B30).

τ_1 and τ_2 can be obtained from Eq. (39). Although it has been derivated for model B, it holds for both models as it is given in terms of the equivalent circuit in Fig. 3*A*.

The frequency responses of the isolated (T) and the embedded transporter (calculated from Eq. 40 and Eq. 41, respectively) are illustrated for the capacitive A model of Fig. 4 (curve "0.5") and for the inductive B model of Fig. 6*k*. Only the amplitude is displayed, because the transporters are minimum-phase networks as shown above (Fig. 8).

The chances of observing nonsteady state behavior of the isolated transporter depend on the ratio

$$\frac{\tau_n}{\tau} = \frac{R_0}{R_0 \| R_t} \tag{43}$$

as R_0 and $R_0 \| R_t$ are the values of the impedance at low and at high frequencies, respectively. Thus, this ratio determines the magnitude of the "wiggle" in the curve labeled "T". (The impedance of the isolated inductive transporter in Fig. 8*B* increases at high frequencies, because of the negative value of R_t in $R_0 \| R_t$.)

If the transporter is embedded in the membrane (Eq. 41), the wiggle becomes less obvious, as the high frequency branch of the curve is bent down by the classical membrane capacitance C_m (curve "M"). Nevertheless, Fig. 8*A* and Fig. 8*B* demonstrate that the deviation of the frequency responses from that of a pure R/C membrane is still well pronounced for the given sets of the parameters of the transporters.

The chances of the occurrence of a clear indication for nonsteady-state properties depend now on the relative locations of τ, τ_1 and τ_2. If τ coincides with τ_1 or τ_2, it is seen from Eq. (41) that only one time constant remains, thus giving the smooth decay of a pure R/C membrane with $\tau_2 = R_0 C_m$ as seen from Eq. (39) if $\tau = \tau_1$ is introduced.

Figure 9 displays the voltage dependences of τ, τ_1, τ_2 and

$$\tau_{RC} = R_0 C_m \tag{44}$$

for 6 sets of reaction constants, which are similar or identical to those used for Figs. 4 to 6. In Figs. 9*a* to 9*d* arrows indicate the membrane potentials, where the distances between the time constants obtain maximum values. At these membrane potentials, optimum chances are provided for the detection of nonsteady-state behavior.

Figure 9 shows that the distance between the slowest time constant τ_1 and τ_{RC} obtains maximum values, when also τ, τ_1 and τ_2 are well separated. This has an important consequence for the experimenter: Very often, the temporal resolution reaches only τ_1, and τ_2 and τ remain hidden in the noise. Nevertheless, the experimenter can realize that τ_1 differs from τ_{RC} which can be calculated from the slope conductance of the steady-state I/V curve and the known value of C_m. This effect was a first hint to a new phenomenon when Gradmann (1975) found a membrane capacitance of $5\,\mu F\,cm^{-2}$ in *Acetabularia*.

The curves in Fig. 9 support what was concluded from the C_t plots in Fig. 4: max-k transporters (Fig. 9*b*) give the best signs of nonsteady-state behavior. The transporter density has to be risen by a factor of 5 in order to give

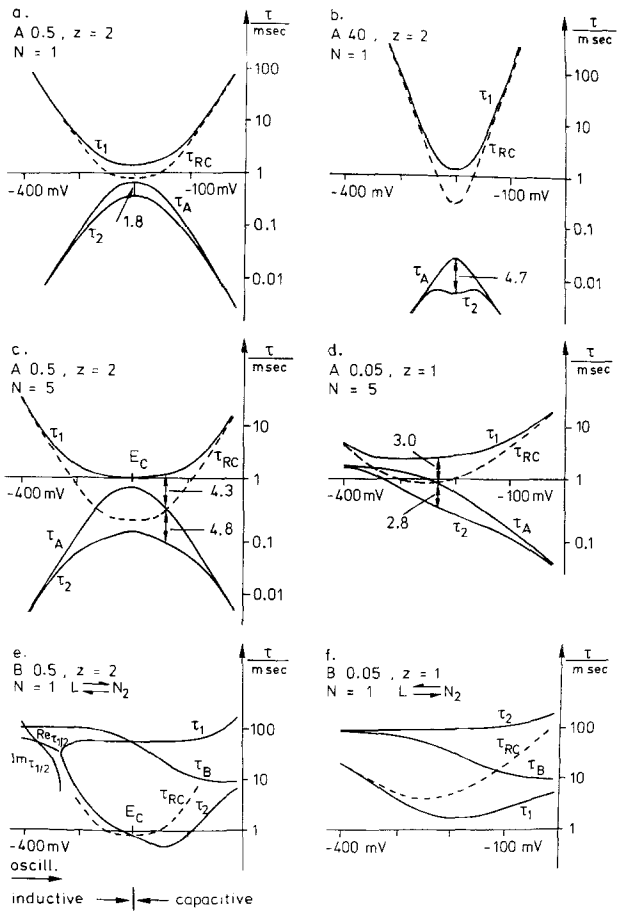

Fig. 9. Synopsis of the voltage dependence of the time constants of Eq. (28): τ (Eq. 15a, b), τ_1 and τ_2 (Eq. 39) and τ_{RC} (Eq. 44) for different sets of the kinetic parameters. Figs. *a*, *c* and *e* correspond to the data set of curve "0.5" in Fig. 4, which displays the double peak in C_t (Fig. 4*f*). 9*a* has the same transporter density as Fig. 4 ($N_0 = 1\,pmol/cm^2$). Only a factor of 1.8 is achieved for the distance between τ_n and τ_2 in model A. $N_0 = 5\,pmol/cm^2$ in Fig. 9*c* gives a better resolution. The values at $-150\,mV$ are used for Fig. 8*A*. Fig. 9*e*: model B creates much greater differences from the data of Fig. 9*a*. Fig. 9*b*: model A with the data of curve "40" in Fig. 3. Fig. 9*d*: model A with the data of Fig. 4 ($z = 1$). Fig. 9*f*: model B with the data of Fig. 9*d*

a good separation of the τ's for max-κ transporters (Figs. 9*d*: $q = 0.05$, *compare* Fig. 9*c* with Fig. 9*a*). Figure 9*d* demonstrates that the transporter with a stoichiometry of $z = 1$ has a chance to be observed, if it is the max-κ type discussed above.

Model B transporters are more effective in creating wide distances between the τ's. Figure 9*e* is the B version of Fig. 9*a*; Fig. 9*f* shows the B version of Fig. 9*d*, but with fivefold smaller N_0. The differences in the τ's can be further enhanced by adequate choice of k_{3L} and k_{L3}. Figure 9*e* displays the phenomenon discussed above: at $-325\,mV$, τ_1 and τ_2 become

complex numbers, thus providing the system with the ability of showing (heavily damped) oscillations.

Exchanging N_1 and N_2 results in symmetrical figures in which the positive sides and negative sides of E_c in Fig. 9*e* and 9*f* are exchanged.

Influence of the Input Port in the Case of Sine Waves

If the experimenter uses sine waves, there is no influence of the choice of the input port (Δv or Δi) on the observability. The distance of the τ's is of similar importance if the inverse function of Eq. (41) is investigated. The frequency responses of impedance and of conductance displayed in a double-logarithmic Bode plot are mirror images of each other.

Step Functions

Step functions have been used already to calculate the responses of the isolated transporter (Eq. 6 and Eq. 11). The calculation of the responses to stepfunctions of the embedded transporter is done by means of Eq. (41) via the inverse Laplace transformation $\mathcal{L}^{-1}$

$$F_{(t)} = \mathcal{L}^{-1}\left\{\frac{1}{p} H_{(p)}\right\} \tag{45}$$

(Milsum, 1966; Riggs, 1966) with $H_{(p)}$ being the impedance function (Eq. 41) if Δi is the input port, or the inverse of Eq. 41 if Δv is the input port.

Completely different curve shapes are obtained for the impedance and the conductance responses, in contrast to sine waves, where the transition from impedance to conductance is easily achieved by an upside-down conversion of Eq. (41) or of Fig. 8.

The response of membrane potential to a step in injected current is shown in Fig. 10 for capacitive and inductive behavior. They are calculated from

$$\Delta v_{(t)} = R_0^* \left\{1 - \frac{\tau_1 - \tau}{\tau_1 - \tau_2} \cdot \exp\left(\frac{-t}{\tau_1}\right) - \frac{\tau_2 - \tau}{\tau_2 - \tau_1} \exp\left(\frac{-t}{\tau_2}\right)\right\} \Delta i \tag{46}$$

(No. 5 in Roberts and Kaufmann, 1966). R_0^* can include the conductances of other transporters as given by Eq. (20).

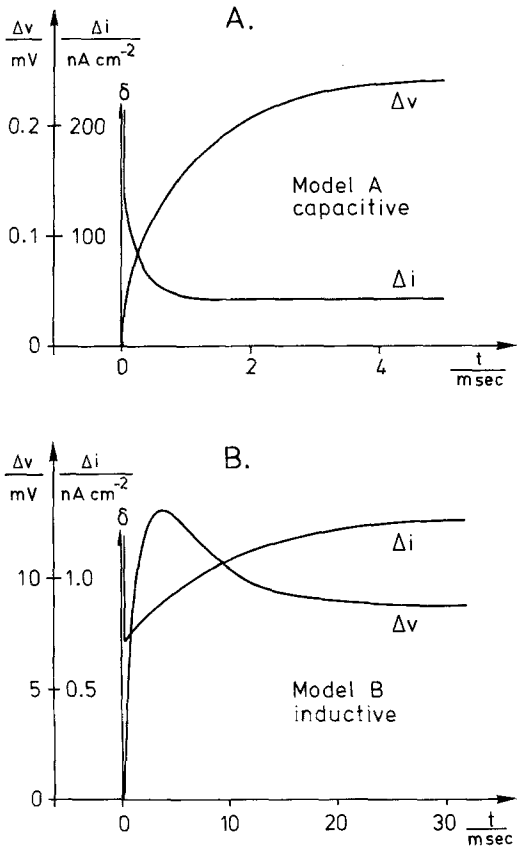

Fig. 10. Responses of the transporter embedded in the membrane and shunted by C_m (Eq. 19, Fig. 3*A*). Δv is the time course of membrane potential caused by a step in membrane current (Eq. 46) (current clamp). Δi is the time course of the current caused by a step in potential (Eq. 47b). The data of the transporters are identical to those used for Figs. 2*A* and 2*B*, which show the Δi responses of the isolated transporter

The time constants seen in the impedance response of Eq. (46) (τ_1 and τ_2) are different from the "real" time constant of the transporter ($\tau = \tau_A$ or τ_B in Eqs. T1-7 or T2-7).

The influence of nonsteady-state behavior on the capacitive response of membrane potential (curve "Δv" in Fig. 10*A*) can be detected only by a computer fit of the measured time course, whereas the overshoot associated to the inductive behavior in Fig. 10*B* (curve "Δv") is a much better indication. Nevertheless, in the case of impedance measurements, sine waves (Fig. 8) give a clearer picture of nonsteady-state behavior.

The response of current to a step in voltage (imposed by a voltage-clamp circuit) is obtained from the insertion of the inverse of Eq. (41) into Eq. (45), after splitting it into its three com-

ponents according to Eqs. (6) and (11) (plus current through C_m)

$$\Delta i_{(t)} = \mathscr{L}^{-1}\left\{\frac{1}{p}\left(p\,C_m + G_0 + \frac{p\,C_t}{1+p\,\tau}\right)\right\}\cdot \Delta v. \quad (47a)$$

This results in

$$\Delta i_{(t)} = \{C_m \delta_{(t)} + G_0 \sigma_{(t)} + G_t \exp(-t/\tau)\}\cdot \Delta v. \quad (47b)$$

$C_m\delta_{(t)}$ is the spike of infinite height which charges C_m in zero time (if the clamp circuit is good enough), $G_0\sigma_{(t)}$ is a step function and nothing else than the current through the slope conductance G_0 according to Ohm's law. The last term witnesses the non steady-state behavior and displays the "correct" time constant.

The time courses of the current response calculated from Eq. (47b) and displayed in Fig. 10 (curves labelled "Δi") display two peculiarities:

At first, the "real" time constant of transporter redistribution shows up in the exp function.

Secondly, non steady-state behavior is no longer masked by the effect of C_m, the classical membrane capacitance.

The elimination of the masking effect is now a technical problem. The theoretically infinitely short time of charging C_m by the δ pulse can be lengthened by insufficient clamp amplifiers, and, probably to a higher degree, by access resistances located between membrane and voltage electrodes. Nevertheless, Eq. (47b) may provide step functions with an advantage over sine waves.

The reason that only the "Δi" curves in Fig. 10 display the "real" time constant τ is as follows: Under open loop conditions, a feedback loop hides the properties of the transporter: The injected current changes membrane potential and thus the distribution of transporter states. This influences the resistance of the transporter which closes the feedback loop by influencing the voltage drop caused by the injected current. The property of feedback loops to mask the intrinsic properties of a system is the reason for using feedback in technical systems. In a voltage-clamp circuit, the electronic feedback loop opens that one of the transporter by preventing the influence of transporter densities on membrane potential.

VIII. Conclusions and Discussion of the Evidence for the Actual Occurrence of Class I Nonsteady-State Behavior

The Problem of Observing Nonsteady-State Behavior in Model A: Density of Transporters

The occurrence of nonsteady-state behavior as manifested by the appearance of an additional capacitance in the electrical impedance of biological membranes can be explained by two different models. Model A is conceptually simpler because its nonsteady-state behavior results from the obviously existing redistribution of states after a change in transport activity.

The problem of model A is the requirement of very high densities of the transporters in the membrane. Even under optimum conditions (curve "40" in Fig. 4) a density of 1 pmol cm^{-2} (or 0.6 transporters per (10 nm)^2) is required for achieving a maximum nonsteady-state capacitance of 3.6 μF/cm^2.

Usefulness of Different Biological Objects for Model A

Transporters with reaction constants similar to those found in *Acetabularia* (Mummert et al., 1981; Gradmann et al., 1982; Hansen et al., 1982) need the fivefold density of transporters for the generation of a C_t of the above value (*see* Fig. 8*A*, Fig. 9*c*, Fig. 10*A*, and Fig. 4 curve "0.5"). These values are obtained from transporters with a stoichiometry of $z=2$ like the Cl_2^{2-} pump in *Acetabularia*.

Pumps with a stoichiometry of $z=1$ like the H^+ pump in *Neurospora* have very little chance of displaying a measurable C_{tA}, because the favorite conditions of Fig. 6 (max-κ type) are very unlikely.

The Benefit of Good Voltage Clamp

There may be a small chance of measuring also small values of C_{tA} in excellent voltage-clamp circuits (e.g. when access resistances are compensated by a negative electronic resistance), where the masking effect of C_m, the biophysical membrane capacitance, is avoided according to Eq. (47b) and Fig. 10 (curves "Δi").

Experimental Evidence for Model A

In spite of the required high transporter densities, model A has been successful in interpret-

ing experimental data. The effect and the predicted voltage dependence of C_{tA} has been found in *Acetabularia*, and the values for the reaction constants obtained from the nonsteady-state analysis were identical to those of the steady-state analysis, even though the approaches are independent (Tittor et al., 1982, 1983).

Zimmermann et al. (1982) interpreted data from *Valonia* on the basis of a model similar to model A. Both investigations resulted in transporter densities equal to that assumed for Fig. 9*c* (5 pmol/cm^{-2}).

Requirements for Model B

Model B can generate high values of C_t without the need of high transporter densities, and thus it may apply to pumps with a stoichiometry of 1:1 or even to channels with high turnover rates and low transporter densities. However, the basic element of model B has not been witnessed so far, even though the reaction scheme proposed by Smith et al. (1980) for the action of vanadate on the (K, Na) pump is similar to the lazy state model in Fig. 1*B*.

The Role of Model B in Regulation

The lazy state is assumed to occur in regulated transport systems. Hansen et al. (*in preparation; see also* Hansen, 1982) use a configuration similar to that of Fig. 1*B* for a model of the control of transport activity via a messenger system by cell metabolism. However, in these investigations, the temporal behavior has been assigned to the messenger system which controls the $N_3 \rightleftharpoons L$ transition.

Weak Hints to the Occurrence of Model B

Experimental evidence for the involvement of model B is not available in that quality as mentioned above for model A. Nevertheless, there are observations which may be regarded as indications of model B. Hyperpolarizing responses showing the curve shape of Fig. 10*B* (curve "Δv") in *Nitella* were reported by Kishimoto (1966) and by Bradley and Williams (1967).

Kishimoto also showed oscillations with periods in the range of seconds, even though they were less damped than expected for model B. Ohkawa and Kishimoto (1974) assumed that a negative resistance was involved in the generation of the hyperpolarizing impulse in *Chara* and they cite several authors who made similar observations in other tissues.

The Stimulus of Searching for Model B

Even though alternative explanations are given in the articles cited above, it may be worthwhile to collect more experimental material regarding the voltage dependence of these phenomena and to test whether the findings are in agreement with the predictions of model B.

In *Characean* cells in which the hyperpolarizing response was observed, OH^- extrusion seems to be subject to regulation. Bisson and Walker (1980) assume a positive feedback action for the stabilization of the alkaline bands. Lucas (1976) showed that an unknown regulatory system couples OH^- extrusion to a locally separated HCO_3^- uptake. Thus OH^- extrusion may be a candidate for a regulated transporter, which generates the observed inductive behavior via a model-B mechanism.

We are grateful to Prof. Dr. Clifford Slayman (New Haven) for very critical reading of this manuscript, and because basic ideas of this approach were created in the stimulating atmosphere of his lab. We are indebted to Mrs. E. Götting who sacrificed weekends to finish the figures in time. This work was supported by the Deutsche Forschungsgemeinschaft (Ha712-7,2, Gr409/7-10). Calculations were done on the PDP10 of the Kieler Rechenzentrum.

Appendix A

Calculation of the Temporal Behavior of a Class I Transporter of Subclass (Model) A (Slow Reaction within the Main Cycle, Fig. 1 A)

A powerful means of describing the temporal behavior also of nonlinear biochemical systems with relatively simple mathematical tools was introduced into the field of biochemistry by Eigen (1968). The so-called relaxation analysis implies that measurements have to be performed along certain guidelines: the system has to be given time to achieve a steady state. Then it is perturbated by a stimulus of such a small amplitude that the response is still in the range of linearity. This procedure is exactly what is applied in the case of impedance measurements. By a voltage-clamp circuit or any other adequate experimental setup, membrane potential is shifted to the desired value. When a steady state is reached, small signals are superposed to the command value, which may be step functions, sine waves or anything else selected for a special purpose. The experimenter has to observe that the output is linear, namely that the response to a sine wave is a sine wave or that the curve shape does not depend on the amplitude.

By means of the tools of relaxation analysis, the response of membrane current Δi to a test change Δv in membrane potential is calculated as follows: In model A, this calculation must not start from Eq. (1), because it holds for steady state only. Instead, the elementary equation

$$i = zF(k_{12}N_1 - k_{21}N_2) = zF(k_{io}r_1N_1 - k_{oi}r_2N_2) \tag{A1}$$

has to be used (Hansen et al., 1981). k_{io}, k_{oi} (Eqs. 2a and b), N_1 and N_2 change with membrane potential. In the case of relaxation analysis, they can be replaced by truncated Taylor series, because of the restriction to linear effects.

$$i = zF\left\{r_1\left(k_{io0} + \frac{dk_{io}}{dv}\Delta v\right)\left(N_{10} + \frac{dN_1}{dv}\Delta v\right) - r_2\left(k_{oi0} + \frac{dk_{oi}}{dv}\Delta v\right)\left(N_{20} + \frac{dN_2}{dv}\Delta v\right)\right\} \tag{A2}$$

with the index 0 indicating steady-state conditions. The introduction of the steady-state condition

$$i - \Delta i = i_0 = zF(r_1k_{io0}N_{10} - r_2k_{oi0}N_{20}) \tag{A3}$$

and of the assumption of linearity

$$r_1\frac{dk_{io}}{dv}\frac{dN_1}{dv}(\Delta v)^2 - r_2\frac{dk_{oi}}{dv}\frac{dN_2}{dv}(\Delta v)^2 \approx 0 \tag{A4}$$

simplifies Eq. (A2):

$$\Delta i = \frac{zF}{u_T}\left\{k_{io}r_1N_{10} + k_{oi}r_2N_{20} + k_{io}r_1\frac{dN_1}{dv} - k_{oi}r_2\frac{dN_2}{dv}\right\}\Delta v. \tag{A5}$$

dk_{io}/dv and dk_{oi}/dv are calculated from Eqs. (2a) and (2b). In the case of k_{io} and k_{oi}, the 0 index is omitted for the sake of simpler expressions, as no confusion can arise from this omission.

N_{10} and N_{20} are steady-state concentrations and thus they can be calculated from the steady-state relationships (Hansen et al., 1981; Gradmann et al., 1982)

$$N_{10} = \frac{k_{oi} + \kappa_{oi}}{r_1K}N_0 \quad \text{and} \quad N_{20} = \frac{k_{io} + \kappa_{io}}{r_2K}N_0 \tag{A6a, b}$$

with

$$K = k_{io} + k_{oi} + \kappa_{io} + \kappa_{oi} \tag{A7}$$

being the sum over all reaction constants.

As r_1 and r_2 are insensitive to membrane potential (they include only voltage-insensitive reactions; Hansen et al., 1981), and as the law of transporter conservation

$$r_1N_1 + r_2N_2 = N_0 \tag{A8}$$

holds, the relationship

$$r_1\frac{dN_1}{dv} = -r_2\frac{dN_2}{dv} \tag{A9}$$

can be introduced into Eq. (A5):

$$\Delta i = \frac{zF}{u_T}\frac{k_{io}(k_{oi} + \kappa_{oi}) + k_{oi}(k_{io} + \kappa_{io})}{K} \cdot N_0 - zF(k_{io} + k_{oi})\frac{dr_2N_2}{dv}\Delta v. \tag{A10}$$

Whereas k_{io} and k_{oi} follow the changes in membrane potential immediately, the change in N_2 and thus in dN_2/dv takes some time as given by Eq. (5):

$$r_2\frac{dN_2}{dt} = (k_{12} + \kappa_{12})N_1 - (k_{21} + \kappa_{21})N_2. \tag{A11}$$

The introduction of the law of transporter conservation, Eq. (A8), leads to

$$r_2\frac{dN_2}{dt} = -r_2KN_2 + (k_{io} + \kappa_{io})N_0. \tag{A12}$$

For linear responses, derivation d/dv of Eq. (A12) leads to (*see* Eq. A2)

$$r_2\frac{d}{dv}\frac{dN_2}{dt} = -r_2\frac{dK}{dv}N_{20} - r_2K\frac{dN_2}{dv} + \frac{dk_{io}}{dv}N_0. \tag{A13}$$

The derivations of the reaction constants are again calculated from Eqs. (2a, b) and d/dv and d/dt can be interchanged as N_2 is a mathematically well-natured function. This converts Eq. (A13) to

$$\frac{r_2}{K}\frac{d}{dt}\frac{dN_2}{dv} = -r_2\frac{dN_2}{dv} + \frac{k_{oi}(k_{io} + \kappa_{io}) + k_{io}(k_{oi} + \kappa_{oi})}{K^2}N_0. \tag{A14}$$

The introduction of the solution of Eq. (A14) for dN_2/dv into Eq. (A10) can be done in different ways. For instance, Eq. (A14) can be solved for a stepwise change in membrane potential Δv:

$$r_2\frac{dN_2}{dv} = \frac{k_{oi}(k_{io} + \kappa_{io}) + k_{io}(k_{oi} + \kappa_{oi})}{K^2} \cdot N_0\{1 - \exp(-t/\tau)\} \tag{A15}$$

with

$$\tau = \frac{1}{K} = \frac{1}{k_{oi} + k_{oi} + \kappa_{oi} + \kappa_{io}} \tag{A16}$$

according to Eq. (A7).

In that case, the response to a stepwise change in membrane potential is obtained from the insertion of Eq. (A16) into Eq. (A10):

$$\Delta i = \frac{zF}{u_T}\frac{k_{io}(k_{oi} + \kappa_{oi}) + k_{oi}(k_{io} + \kappa_{io})}{K} \cdot N_0\Delta v_0\left\{1 - \frac{k_{io} + k_{oi}}{K}(1 - \exp(-t/\tau))\right\} \tag{A17}$$

with Δv_0 being the magnitude of the step in potential.

A more general approach which applies to any kind of input signal is given by the operational method (Capellos & Bielski, 1972) which is based on the Laplace transformation of Eq. (A14) (Riggs, 1966)

$$r_2\frac{\overrightarrow{dN_2}}{dv} = \frac{k_{io}(k_{oi} + \kappa_{oi}) + k_{oi}(k_{io} + \kappa_{io})}{K^2}N_0\frac{1}{1 + p\tau}. \tag{A18}$$

which converts Eq. (A10) to (arrows indicate complex amplitudes)

$$\overrightarrow{\Delta i} = \frac{zF}{u_T}N_0\frac{k_{io}(k_{oi} + \kappa_{oi}) + k_{oi}(k_{io} + \kappa_{io})}{K} \cdot \left\{1 - \frac{k_{io} + k_{oi}}{K}\frac{1}{1 + p\tau}\right\}\overrightarrow{\Delta v} \tag{A19a}$$

$$= \frac{zFN_0}{u_T} \frac{\{k_{io}(k_{oi}+\kappa_{oi})+k_{oi}(k_{io}+\kappa_{io})\}(\kappa_{io}+\kappa_{oi})}{K^2}$$

$$\cdot \frac{1+p/(\kappa_{io}+\kappa_{oi})}{1+p\tau} \overrightarrow{\Delta v}. \tag{A19b}$$

The Equivalent Circuit of Model A

From Eq. (A19), the complex conductance of the transporter can be calculated

$$\vec{G} = \frac{\overrightarrow{\Delta i}}{\overrightarrow{\Delta v}} = G_0 \cdot \frac{1+p/(\kappa_{io}+\kappa_{oi})}{1+p/K} \tag{A20}$$

with

$$G_0 = \frac{zF}{u_T} N_0 \frac{k_{io}(k_{oi}+\kappa_{oi})+k_{oi}(k_{io}+\kappa_{io})(\kappa_{io}+\kappa_{oi})}{K^2}. \tag{A21}$$

Derivation d/dv of Eq. (1) shows that G_0 is nothing else than the steady-state slope conductance of the transporter. This value of G is obtained from Eq. (A20) for very low frequencies or d-c-measurements ($p=0$). p is the generalized frequency, which is in the case of sinusoidal test signals

$$p = 2\pi f \sqrt{-1} \tag{A22}$$

with f being the frequency.

The electrical impedance is the inverse of the conductance

$$\vec{R} = R_0 \frac{1+p/K}{1+p/(\kappa_{io}+\kappa_{oi})} \tag{A23}$$

with

$$R_0 = \frac{1}{G_0} = \left.\frac{dv}{di}\right|_{\text{steady-state}} \tag{A24}$$

being the steady-state membrane impedance.

The equivalent circuit of Fig. 3*A* has the same impedance function

$$\vec{R} = R_0 \frac{1+p\,C_t R_t}{1+p\,C_t(R_t+R_0)}. \tag{A25}$$

The comparison of Eqs. (A23) and (A25) enables the interpretation of the results of electrical measurements of transport activity (which are naturally obtained in terms of equivalent circuits) in terms of the reaction kinetic constants of the transport molecule

$$\tau_A = \frac{1}{K} = \frac{1}{k_{oi}+k_{io}+\kappa_{oi}+\kappa_{io}} = C_t R_t \tag{A26}$$

$$\tau_{nA} = \frac{1}{\kappa_{io}+\kappa_{oi}} = C_t(R_t+R_0) \tag{A27}$$

and $R_0 = 1/G_0$ as given by Eq. (A21). From Eqs. (A26), (A27) and (A21), the equations of Table 1 are calculated.

Appendix B

Calculation of the Electrical Impedance of a Class I Transporter with Lazy State (Model B in Fig. 1B), Slowly Equilibrating with the Fast Main Cycle

In Fig. 1*D*, a "lazy" state L is connected to state N_3 of the transport cycle. Transporters in state L do not contribute to transport. Thus in model B, N_0 in Eq. (1) has to be replaced by $N_0 - L$:

$$i = zF \frac{k'_{io}\kappa'_{oi} - k'_{oi}\kappa'_{io}}{K'}(N_0 - L) = zF\, w^0(N_0 - L) \tag{B1a, b}$$

with

$$K' = k'_{io} + k'_{oi} + \kappa'_{io} + \kappa'_{oi}. \tag{B2}$$

w' is defined by the comparison of Eq. (B1a) and Eq. (B1b). The reaction constants are labeled by an apostrophe in order to indicate that something is missing. The '-reaction constants are related to the reserve factors r'_1 and r'_2 which do not include the reserve factors r_{1L} and r_{2L} related to the L state. This is illustrated by the following set of equations:

$$r'_1 = r_1 - r_{1L}, \qquad r'_2 = r_2 - r_{2L} \tag{B3a, b}$$

$$s_1 = \frac{r'_1}{r_1}, \qquad s_2 = \frac{r'_2}{r_2} \tag{B4a, b}$$

$$k'_{oi} = \frac{k_{21}}{r'_2} = \frac{k_{21}}{s_2 r_2} = \frac{k_{oi}}{s_2} \tag{B5a}$$

$$k'_{io} = \frac{k_{12}}{r'_1} = \frac{k_{12}}{s_1 r_1} = \frac{k_{io}}{s_1} \tag{B5b}$$

$$\kappa'_{oi} = \frac{\kappa_{21}}{r'_2} = \frac{\kappa_{21}}{s_2 r_2} = \frac{\kappa_{oi}}{s_2} \tag{B5c}$$

$$\kappa'_{io} = \frac{\kappa_{12}}{r'_1} = \frac{\kappa_{12}}{s_1 r_1} = \frac{\kappa_{io}}{s_1}. \tag{B5d}$$

s_1, s_2, r_{1L} and r_{2L} are voltage insensitive, as they are related to the neutral limb, but not time invariant as transient deviations from steady-state concentrations can occur after a change in membrane potential. In model B, the slow time constant is associated with the exchange of L with the transport cycle via N_3. Equilibration within the cycle is assumed to be rapid. Thus, in contrast to model A, the response of current can be calculated from Eq. (B1). As in the case of Eq. (A2), the methods of relaxation analysis are applied which provide the response of the current, Δi, in the linear range

$$\Delta i = zF(N_0 - L)_0 \frac{dw}{dv}\Delta v - zF\, w_0 \frac{dL}{dv}\Delta v. \tag{B6}$$

The first term is the initial response, which looks similar to the steady-state response. However, it is not a steady-state response as L changes with time and the second term starts to grow. L can be independent of membrane potential, if N_3 is in the "reaction kinetic middle" between N_1 and N_2 ($s_1 = s_2$).

The individual terms of Eq. (B6) are calculated as follows: The application of Eqs. (B4a, b) and (B5a to d) results in

$$N_0 - L_0 = r_1' N_1 + r_2' N_2$$
$$= \frac{s_1(k_{oi}+\kappa_{oi}) + s_2(k_{io}+\kappa_{io})}{K} N_0. \quad \text{(B7a, b)}$$

dw'/dv is obtained from the derivation of w in Eq. (B1b):

$$\frac{dw'}{dv} = \frac{1}{u_T} \frac{k_{io}'(k_{oi}'+\kappa_{oi}') + k_{oi}'(k_{io}'+\kappa_{io}')(\kappa_{io}'+\kappa_{oi}')}{K'^2}. \quad \text{(B8a)}$$

The apostrophe labels the parameters of the L-free transporter according to the definitions of Eqs. (B3) to (B5). The actual observed reaction constants of the complete transporter can be introduced by means of Eqs. (B4) and (B5) as in the case of Eq. (B7b).

$$\frac{dw'}{dv} = \frac{1}{u_T} \frac{k_{io}(k_{oi}+\kappa_{oi}) + k_{oi}(k_{io}+\kappa_{io})(s_2\kappa_{io} + s_1\kappa_{oi})}{(K_s)^2} \quad \text{(B8b)}$$

with

$$K_s = s_2(k_{io}+\kappa_{io}) + s_1(k_{oi}+\kappa_{oi}). \quad \text{(B9)}$$

Introducing Eqs. (B7b), (B8b) and (B1b) (in order to replace w_o' by i_o) converts Eq. (B6) to

$$\Delta i = \left\{ \frac{zFN_0}{u_T} \frac{(k_{io}(k_{oi}+\kappa_{oi}) + k_{oi}(k_{io}+\kappa_{io})(s_2\kappa_{io}+s_1\kappa_{oi})}{K \cdot K_s} - \frac{i_0}{N_0 - L_0} \frac{dL}{dv} \right\} \Delta v. \quad \text{(B10)}$$

Without the lazy state L ($s_2 = s_1 = 1$), the first term is identical to the constant factor in Eq. (A19b), which is G_0, the steady-state conductance. This is correct, as in model B, equilibration within the cycle is assumed to be very fast.

The temporal behavior of L is given by

$$\frac{dL}{dt} = k_{3L} N_3 - k_{L3} L. \quad \text{(B11)}$$

The transporters coming out of L into N_3 spread around the cycle, because equilibration within the cycle of model B ($N_1 - N_2 - N_3$) is assumed to be faster than the $N_3 - L$ exchange. The ratio of transporters staying in N_3 to those in the whole cycle ($N_0 - L$) is called ρ.

$$N_3 = \rho(N_0 - L) = r_{13} N_1 + r_{23} N_2$$
$$= \frac{r_{13}(k_{oi}'+\kappa_{oi}')}{r_1' K'} + \frac{r_{23}(k_{io}'+\kappa_{io}')}{r_2' K'} (N_0 - L) \quad \text{(B12a, b, c)}$$

with

$$r_{13} = \frac{\kappa_{13}}{\kappa_{31}+\kappa_{32}} \quad \text{and} \quad r_{23} = \frac{\kappa_{23}}{\kappa_{31}+\kappa_{32}} \quad \text{(B13a, b)}$$

being the reserve factors relating N_3 to N_1 and N_2.

Introducing Eq. (B12a) into Eq. (B11) leads to

$$\frac{dL}{dt} = \rho k_{3L}(N_0 - L) - k_{L3} L = -(\rho k_{3L} + k_{L3}) L + \rho k_{3L} N_0. \quad \text{(B14a, b)}$$

Derivation d/dv of Eq. (B14) is performed along the same rules as in the case of Eq. (A12):

$$\tau \frac{d}{dt} \frac{dL}{dv} = -\frac{dL}{dv} + \frac{k_{3L}(N_0 - L_0)}{k_{3L}\rho + k_{L3}} \frac{d\rho}{dv} \quad \text{(B15)}$$

with

$$\tau = \frac{1}{\rho k_{3L} + k_{L3}}. \quad \text{(B16)}$$

The comparison of Eq. (B12a) with Eq. (B12c) provides the explicit expression for ρ

$$\rho = \frac{\frac{r_{13}}{r_1}(k_{oi}+\kappa_{oi}) + \frac{r_{23}}{r_2}(k_{io}'+\kappa_{io}')}{K_s}. \quad \text{(B17)}$$

Derivation d/dv leads to

$$\frac{d\rho}{dv} = \frac{\left(\frac{r_{23}}{r_2} - \frac{r_{13}}{r_1}\right)(k_{oi}(k_{io}+\kappa_{io}) + k_{io}(k_{oi}+\kappa_{oi})}{u_T (K_s)^2}. \quad \text{(B18)}$$

Again, Eqs. (B4) and (B5) are used to eliminate the L-free (apostrophe-labeled) parameters.

r_{23}/r_2 can be replaced as follows:

$$\frac{r_{23}}{r_2} = \frac{N_3}{r_2 N_2} = \frac{k_{3L} L}{k_{L3} r_2 N_2}$$
$$= \frac{k_{L3}}{k_{3L}} \frac{r_{2L}}{r_2} = \frac{k_{L3}}{k_{3L}}(1 - s_2). \quad \text{(B19a, b, c, d)}$$

In Eq. (B19), the definition of r_{23}, the steady state of Eq. (B11), the definition of r_{2L}, and Eqs. (B3) and (B4) are used. Eq. (B19d) converts the first factor of Eq. (B18) to

$$\frac{r_{23}}{r_2} - \frac{r_{13}}{r_1} = \frac{k_{L3}}{k_{3L}}(s_1 - s_2). \quad \text{(B20)}$$

The product of k_{L3}/k_{3L} with the ratio of reaction constants in Eq. (B15) is

$$\frac{k_{L3}}{k_{3L}} \frac{k_{3L}}{k_{3L}\rho + k_{L3}} = 1 - \frac{\rho k_{3L}}{k_{3L}\rho + k_{L3}} = \frac{N_0 - L_0}{N_0} = \frac{K_s}{K}. \quad \text{(B21a, b)}$$

For Eq. (B21b), the steady-state solution of Eq. (B14b) is used and Eq. (B21c) is obtained by means of Eq. (B7b). The introduction of Eqs. (B18), (B20) and (B21c) converts Eq. (B15) to

$$\frac{d}{dt} \frac{dL}{dv} = -\frac{dL}{dv} + \frac{dL_0}{dv} \quad \text{(B22)}$$

with

$$\frac{dL_0}{dv} = \frac{N_0 - L_0}{u_T} \frac{\{(k_{io}(k_{oi}+\kappa_{oi}) + k_{oi}(k_{io}+\kappa_{io})\}(s_1 - s_2)}{K K_s} \quad \text{(B23)}$$

being the steady-state dependence of L on membrane potential.

At this point, a test of the above calculations may be desirable: The steady-state solution of Eq. (B22), namely Eq. (B23), which is obtained by zeroing the left-hand side of Eq. (B22) should yield the steady-state conductivity of model A (Eq. A21), as model A and model B are both Class I transporters which must not show differences in steady-state behavior

$$\Delta i_\infty = \frac{N_0 z F}{u_T} \frac{(k_{io}(k_{oi}+\kappa_{oi}) + k_{oi}(k_{io}+\kappa_{io})}{K K_s} Q \Delta v_\infty \quad \text{(B24)}$$

with

$$Q = s_1\kappa_{oi} + s_2\kappa_{io} - \frac{(k_{io}\kappa_{oi} - k_{oi}\kappa_{io})(s_1 - s_2)}{K_s}$$

$$= \frac{K_s(\kappa_{io} + \kappa_{oi})}{K}. \qquad \text{(B25a, b)}$$

Q is calculated from the insertion of the steady-state solution of Eq. (B22) into (B6).

The insertion of Eq. (B25b) into Eq. (B24) shows that, indeed, the quotient $\Delta i_\infty/\Delta v_\infty$ is identical with G_0 of Eq. (A21). The nonsteady-state solution is similar to that of Eq. (A14), because Eqs. (A14) and (B22) are both first-order differential equations. Thus the solution of Eq. (B6) is

$$\Delta i = \frac{k_{io}(k_{oi} + \kappa_{oi}) + k_{oi}(k_{io} + \kappa_{io})}{u_T \cdot K \cdot K_s}$$

$$\cdot \{zFN_0(s_1\kappa_{oi} + s_2\kappa_{oi}) - i_0(s_1 - s_2)y\}\,\Delta v \qquad \text{(B26)}$$

with

$$y_{(t)} = 1 - \exp(-t/\tau_B) \qquad \text{(B27a)}$$

for a stepwise change in v and

$$y_{(p)} = \frac{1}{1 + p\tau_B} \qquad \text{(B27b)}$$

if the operational method is applied (Riggs, 1966). τ_B is given by Eq. (B16), $p = 2\pi f\sqrt{-1}$ (Eq. A22) if sine waves are used, i_0 replaces w_0 by means of Eqs. (B1b) and (1), modified for apostrophe-free reaction constants.

The transfer function, which is obtained from Eq. (B26) if the operational solution is introduced is rearranged to a more familiar form

$$\overrightarrow{\Delta i} = G_0 \frac{1 + p\tau_{nB}}{1 + p\tau_B}\overrightarrow{\Delta v}. \qquad \text{(B28)}$$

The value of τ_{nB} is obtained from the following conversions of Eq. (B26)

$$\overrightarrow{\Delta i} = \frac{G_0}{Q}\left(a + \frac{b}{1 + p\tau_B}\right)\overrightarrow{\Delta v} = G_0 \frac{1 + \frac{a\tau_B}{a+b}p}{1 + p\tau_B}\overrightarrow{\Delta v} \qquad \text{(B29a, b)}$$

with a and b identified by the comparison of Eq. (B28) with Eq. (B26). $a + b = Q$ of Eq. (B25). The comparison of Eq. (B28) with Eq. (B29b) yields

$$\tau_{nB} = \frac{s_1\kappa_{oi} + s_2\kappa_{io}}{\kappa_{oi} + \kappa_{io}} \cdot \frac{K}{K_s}\tau_B \qquad \text{(B30)}$$

with τ_B given by Eq. (B16), and K and K_s by Eqs. (A7) and (B9), respectively.

The Equivalent Circuit of Model B

Eq. (B28) is similar to Eq. (A19b). This implies that the same equivalent circuit (Fig. 3*A*) applies to model A and to model B.

For model B, the elements are related to the parameters of the transporter as follows: $G_o = 1/R_0$ is the steady-state slope conductance as shown by means of Eq. (B25b). It is no surprise that G_0 of model A and G_0 of model B, given by Eq. (A21), are identical, as model A and model B cannot be distinguished by steady-state measurements.

$G_t = 1/R_t$ is the scaling factor of y in Eq. (B26). The explicit expression is given by Eqs. (T2-5) and (T2-6). C_t can be calculated from the relationship

$$\tau_B = C_t \cdot R_t. \qquad \text{(B31)}$$

It is given by Eqs. (T2-3) and (T2-4).

τ_{nB} of Eq. (B28) is related to the elements of the equivalent circuit as follows

$$\tau_{nB} = C_t \cdot (R_t + R_0). \qquad \text{(B32)}$$

This relationship is obtained from the comparison of Eq. (B28) with the inverse of Eq. (A25).

References

Benz, R., Läuger, P. 1976. Kinetic analysis of carrier-mediated ion transport by the charge-pulse technique. *J. Membrane Biol.* **27**:171–191

Bisson, M.A., Walker, N.A. 1980. The *Chara* plasmalemma at high pH. Electrical measurements show rapid specific passive uniport of H^+ or OH^-. *J. Membrane Biol.* **56**:1–7

Blinks, L.R., Skow, R.K. 1941. The electrical capacity of *Valonia*. Direct current measurements. *J. Gen. Physiol.* **24**:247–262

Bode, H.W. 1964. Network Analysis and Feed-back Amplifier Design. Chap. XIV. D. Van Nostrand, Princeton, N.J.

Bradley, J., Williams, E.J. 1967. Voltage-controllable negative differential resistance in *Nitella translucens*. *Biochim. Biophys. Acta* **135**:1078–1080

Capellos, C., Bielski, B.H.J. 1972. Kinetic Systems. Wiley-Interscience, New York

Cole, K.S. 1968. Membranes, Ions and Impulses. University of California Press

Coster, H.G.L. 1965. A quantitative analysis of voltage-current relationships of fixed charge membranes and the associated property of "punch through." *Biophys. J.* **5**:669–686

Coster, H.G.L. 1973. The douple fixed charge membrane. Low frequency dielectric dispersion. *Biophys. J.* **13**:118–132

Curtis, H.J., Cole, K.S. 1937. Transverse electric impedance of *Nitella*. *J. Gen. Physiol.* **21**:189–201

Curtis, H.J., Cole, K.S. 1938. Transverse electric impedance of the squid giant axon. *J. Gen. Physiol.* **21**:757

Eigen, M. 1968. New looks and outlooks on physical enzymology. *Q. Rev. Biophys.* **1**:3

Findlay, G.P. 1970. Membrane electrical behavior in *Nitellopsis obtusa*. *Aust. J. Biol. Sci.* **23**:1033–1045

Gradmann, D. 1975. Analog circuit of the *Acetabularia* membrane. *J. Membrane Biol.* **25**:183–208

Gradmann, D., Hansen, U.P., Slayman, C.L. 1982. Reaction-kinetic analysis of current-voltage relationships for electrogenic pumps in *Neurospora* and *Acetabularia*. *In:* Electrogenic Ion Pumps. C.L. Slayman, editor. *Curr. Top. Membr. Transp.* **16**:257–276. Academic Press, New York

Hansen, U.-P. 1982. Kinetic analysis of regulation of membrane transport. *In:* Membranes and Transport. A. Martonosi, editor. pp. 639–644. Plenum Press, New York

Hansen, U.-P., Gradmann, D., Sanders, D., Slayman, C.L. 1981. Interpretation of current-voltage relationships for "active" ion transport systems: I. Steady-state reaction-

kinetic analysis of Class-I mechanisms. *J. Membrane Biol.* **63**:165–190

Hansen, U.P., Gradmann, D., Tittor, J., Sanders, D., Slayman, C.L. 1982. Kinetic analysis of active transport: Reduction models. *In:* Plasmalemma and Tonoplast: Their Functions in the Plant Cell. D. Marmé, E. Marrè, and R. Hertel, editors. pp. 77–84. Elsevier Biomedical, Amsterdam

Inoue, I., Ishima, Y., Horie, H. 1971. Properties of excitable membrane produced on the surface of protoplasmic drop in *Nitella. Proc. Jpn. Acad.* **47**:549–553

Kishimoto, U. 1966. Hyperpolarizing response in *Nitella* internodes. *Plant Cell Physiol.* **7**:429–439

Kishimoto, U. 1974. Transmembrane impedance of the *Chara* cell. *Jpn. J. Physiol.* **24**:403–417

Kishimoto, U., Kami-ike, N., Takeuchi, Y., Ohkawa, T. 1982. An improved method for determining the ionic conductance and capacitance of the membrane of *Chara corallina. Plant Cell Physiol.* **23**:1041–1054

Kolb, H.-A., Frehland, E. 1980. Noise-current generated by carrier mediated ion-transport at non-equilibrium. *Biophys. Chem.* **12**:21–34

Kolb, H.-A., Läuger, P. 1978. Spectral analysis of current noise generated by carrier-mediated ion transport. *J. Membrane Biol.* **41**:167–187

Läuger, P. 1980. Kinetic properties of ion carriers and channels (*Topical Review*). *J. Membrane Biol.* **57**:163–178

Lucas, W.J. 1976. Plasmalemma transport of HCO_3^- and OH^- in *Chara corallina:* Non-antiporter systems. *J. Exp. Bot.* **27**:19–31

Matsumoto, N., Inoue, I., Kishimoto, U. 1970. The electrical impedance of squid axon membrane measured between internal and external electrodes. *Jpn. J. Physiol.* **20**:516–526

Milsum, J.H. 1966. Biological Control Systems Analysis. McGraw Hill, New York

Mummert, H., Hansen, U.P., Gradmann, D. 1981. Current-voltage curve of electrogenic Cl^- pump predicts voltage-dependent Cl^- efflux in *Acetabularia. J. Membrane Biol.* **62**:139–148

Ohkawa, T., Kishimoto, U. 1974. The electromotive force of the *Chara* membrane during the hyperpolarizing response. *Plant Cell Physiol.* **15**:1039–1054

Riggs, D.S. 1966. Control Theory and Physiological Feed-Back Mechanisms. The Williams and Wilkins Co., Baltimore

Roberts, G.E., Kaufmann, H. 1966. Table of Laplace transforms. W.B. Saunders, Philadelphia and London

Sandblom, J., Walker, J.L., Jr., Eisenman, G. 1972. The transient response and impedance locus of a mobile site membrane. *Biophys. J.* **12**:587–596

Sanders, D., Hansen, U.-P. 1981. Mechanism of Cl^--transport at the plasma membrane of *Chara corallina.* II. Transinhibition and the determination of H^+/Cl^- binding order from a reaction kinetic model. *J. Membrane Biol.* **58**:139–153

Sanders, D., Hansen, U.-P., Slayman, C.L. 1981. Role of the plasma membrane proton pump in pH regulation in non-animal cells. *Proc. Natl. Acad. Sci. USA* **78**:5903–5907

Skierczynska, J., Spiewla, E., Zolnierczuk, R., Bulanda, W., Wardak, A. 1973. The measurement of the membrane resistance of Characeae by alternating and direct currents. *J. Exp. Bot.* **24**:1015–1023

Smith, R.L., Zinn, K., Cantley, L.C. 1980. A study of the vanadate-trapped state of the (Na, K)-ATPase. *J. Biol. Chem.* **255**:9852–9859

Thomas, R.C. 1978. Ion-sensitive intracellular microelectrodes. Academic Press, London, New York, San Francisco

Tittor, J., Hansen, U.-P., Gradmann, D. 1983. Impedance of the electrogenic Cl^- pump in *Acetabularia:* Electrical frequency entrainements, voltage-sensitivity, and reaction-kinetic interpretation. *J. Membrane Biol.* **75**:129–139

Tittor, J., Hansen, U.-P., Gradmann, D., Martensen, H.J. 1982. Non-steady state kinetic behavior of Class I transport systems observed as "pump capacitance" in electrical impedance of biological membranes. *Hoppe Seyler's Z. Physiol. Chem.* **363**:908

Zimmermann, U., Büchner, K.-H., Benz, R. 1982. Transport properties of mobile charges in algal membranes: Influence of pH and turgor pressure. *J. Membrane Biol.* **67**:183–197

Received 10 September 1982; revised 14 February 1983